10. Special Finite Elements for Continua

10.1 Requirements for Continuum Finite Elements

The search for finite elements which can be applied to arbitrary problem classes within solid mechanics has a long history. This can be seen from the numerous scientific papers devoted to this topic. Main target of a development of finite elements is summarized in the following enumeration.

1. *Locking* free behaviour for incompressible materials,
2. good bending performance,
3. no *locking* in thin elements,
4. no sensitivity against mesh distortions,
5. good coarse mesh accuracy,
6. simple implementation of nonlinear constitutive equations and
7. efficiency (e.g. few necessary integration points).

These points result from different demands and can also lead to different element formulations.

The first point is associated with the numerical simulation of a special problem classes which include in solid mechanics rubber like materials and elasto-plastic material equations in the framework of J_2-plasticity. During the last years, different special finite elements were developed for this applications. This results from the fact that classical low order displacement elements, which were described in Chap. 4, are not sufficient. The constraint related to the incompressible behaviour leads even for geometrical linear elements to *locking*, see e.g. Braess (2007), Zienkiewicz and Taylor (1989) and Hughes (1987). Finite elements which are suitable for incompressible materials will be described in detail in Sects. 10.2, 10.4 and 10.5.

The second and third points are of significance when three-dimensional solid elements shall be employed to solve beam- or shell problems since beam and shell structures are often dominated by bending behaviour and are, by construction, thin in one or two spatial coordinated. Using three-dimensional elements allow a simple implementation of three-dimensional constitutive equations which is not so easily possible when classical beam or shell models are used. Furthermore, the treatment of finite rotations are avoided by such formulations, see Sect. 9.4.

The fourth point is essential when modern methods for mesh generation are employed. These methods lead for arbitrary geometries to so-called unstructured meshes which consist of finite elements shapes with arbitrary geometry, see e.g. Figs. 8.7, 8.8, 8.9, 8.10, 8.11, 8.12, 8.13, 8.14, 8.15. Another source for the distortion of finite elements is the change of the nodal coordinates during a nonlinear simulations which can lead to severely deformed finite elements.

The fifth point is related to the fact that in real engineering applications often three-dimensional components have to be analysed which size and complexity cannot be modeled using a converged mesh, especially when the simulation is nonlinear. Hence there is still need for elements which depict a good accuracy, even when used within a coarse mesh. Of course, the importance of this point will diminish with the increasing computing power, but at the moment it is still of concern.

The sixth point follows from the fact that more accurate mathematical and physical models have to be used within the simulation of nonlinear engineering structures. Within this process, new complex nonlinear constitutive equations have to be implemented. Here a simple interface to the finite element should support the user in order to efficiently change existing finite elements and to be able to implement new complex constitutive equations.

Finally, it can be mentioned that efficiency is not only related to speed of the element formulation but also to the memory requirement. The latter demand is essential when e.g. inelastic problems with several hundred thousand or millions of finite element have to be solved within a given time frame. This speed of the element formulation is essential when iterative solvers are applied since in that case the time for the computation of residuals and tangent matrices is of the same order as the time used by the solver within one iteration.

New developments show that finite elements with a high order of interpolations (so-called p-version of finite elements) can be applied successfully to finite deformation problems for rubber-like materials, see Heisserer et al. (2007).

Low order finite elements have been proven to be robust for many nonlinear simulations. This has to do with a low regularity of the analytical solution which can exclude higher order interpolations, see also Sect. 8.1. A further fact which supports lower order elements is the sparsity of the global tangent matrices since low order elements yield a smaller bandwidth. Due to that the global equation system can be solved more efficiently, which is crucial for the simulation of large systems. In case of numerical simulations which include inelastic material behaviour, one or more history variables have to be stored per integration point. As an example, a problem with J_2 plasticity is considered to obtain the variation of $\boldsymbol{F}_e$ for the ansatz (10.88), see Sect. 6.2.2, in which six plastic strain components have to be stored per integration point. This leads to the memory requirement for storing the history variables when a finite element mesh of a cube with 10^6 finite elements is used which is shown in Table 10.1. The memory requirement is

Table 10.1: Memory requirement for history variables for 10^6 finite elements

Order of interpolation	Number of GAUSS-points	Memory requirement
1	1	56 MByte
1	8	448 MByte
2	27	1512 MByte

larger when iterative solvers or special direct sparse solvers are used, see Sect. 5.2, but is basically of the same order of magnitude. Hence it is advantageous to use elements with a minimum number of integration points in order to optimize memory requirement. Of course, one has to be careful to compare linear and quadratic or other higher order elements since the elements with higher order have a higher order of convergence when the solution has the necessary regularity, see Sect. 8.1. In that case, less finite elements of higher order can be used which yields results with the same accuracy. (Assume that half of the elements per side are sufficient for the discretization of the above cube, then the memory requirement for the history variables reduces for quadratic elements to 189 MByte.) However, in order to compare the finite element discretizazions of different interpolation orders, the total solution time needed to obtain a result with the same accuracy has to be considered.

The memory requirement for history variables play an essential role when explicit integrations schemes are employed to simulate impact or shock problems. Here only the residual has to be stored, see Sect. 6.1.1, which leads to the storage of three values per node. In that case, the storage requirement for the example above is roughly $3 \times 101^3 = 3.091 \times 10^6$ values for the residual vector. The number of history variables for the correct two-point GAUSS-integration in each coordinate direction amounts to $2 \times 2 \times 2 \times 10^3 = 8 \times 10^6$. This is more than double of the storage needed for the residual vector. In order to reduce the overall computing time, all quantities have to be retained in the main memory. In such case, the storage of the history variables is a major concern for explicit computations. Hence most of the explicit finite element codes use specially stabilized finite elements with only one-GAUSS-point. This formulation will be discussed in Sect. 10.4.

It is well known that the pure displacement element with bilinear or trilinear ansatz function has bad convergence behaviour in bending problems, especially if the length in one direction is a lot smaller than in the other ones, e.g. for beam or shell structures. Hence special elements were developed for such problems. With such elements, which is still based on linear ansatz functions, the convergence order cannot be increased with regard to (8.6) or (8.10), but the constant C is reduced considerably. Thus the required accuracy of the finite element solution can be achieved with considerably less elements. In this connection, the ideal element would be an element which is well performing for bending as well as for incompressible problems.

Different formulations have been developed in order to construct finite elements which fulfil all seven requirements stated above. These are:

- techniques which base on a reduced integration of the integrals leading to the element matrices,
- stabilization methods,
- hybrid or mixed variational principles which base on complimentary energy written in terms of the stress field,
- mixed variational principle of HU–WASHIZU type,
- mixed variational principle for rotational fields,
- mixed variational principle for special quantities,
- nodally based elements,
- composite or macro formulations for the element,
- higher order displacement elements and
- formulations based on the COSSERAT point theory.

In the following, different possibilities are summarized and their differences are discussed. After that some of the techniques are presented in detail.

1. **Reduced integration and stabilization.** The most simple method is the "reduced integration" of the integrals leading to the finite element vectors and matrices. It is also very efficient and safes memory for history data storage since less integration points are used. Underintegration or reduced integration means that less GAUSS points are used for the integration of tangent matrices and residual vectors than necessary for the chosen polynomial degree of the shape functions, for first applications see e.g. Zienkiewicz et al. (1971). This reduced integration was developed to avoid *locking* in case of incompressibility. In that case, it is often only applied to the pressure part of the constitutive equation, see e.g. Malkus and Hughes (1978), Hughes (1980) and Sect. 10.2. For reduced integration techniques exist many variants. This stems from the fact that reduced integration is always associated with a rank deficiency of the tangent matrices which is cured by different methods. The related methods are generally known as stabilization techniques. A literature review regarding this topic is presented in Sect. 10.4, in which stabilization techniques from Belytschko et al. (1984) are presented. Using the reduced integration together with stabilization leads to finite elements which fulfil conditions 1, 4, 5, 6 and 7. These elements are *locking* free in case of incompressibility, they have a good coarse mesh accuracy; they are not sensitive against mesh distortions and can be used for arbitrary constitutive equations. The reduced integration provides the most efficient possibility to compute the element residual and the element tangent stiffness (e.g. for an eight-node brick element, only one GAUSS point is needed). However, these elements need the choice of artificial stabilization parameters. In the worst case, e.g. for some bending problems, the finite element solution

can directly depend on the stabilization parameter, see also Sect. 10.4. However, new developments show improvements, see e.g. Reese (2005).

2. **Hybrid or mixed variational principles.** When mixed variational principles are used as basis for finite element discretization, different possibilities exist for the construction of the finite element matrices. This is related to the many different existing mixed forms. Some of them need conforming displacement fields together with non-conforming stress or strain fields, others rely on conforming stress fields but allow non-conforming displacement fields. Theoretical background for linear mixed methods can be found in Washizu (1975) and in various monographs and papers, for the mathematical literature, see e.g. Braess (2007) and Brenner and Scott (2002). For the case of linear elasticity, hybrid elements where first described in Pian (1964) which has lead to many different finite element formulations up to now. Within this approach, Pian and Sumihara (1984) developed a finite element which is efficient and accurate. However due to the need to invert the constitutive equations within the formulation in order to obtain the constitutive equations in terms of the stress field, there are only few elements for St. Venant materials known which work for large deformations. A special formulation for Neo–Hooke materials will be presented in Sect. 10.3.
3. **Enhanced strain elements based on the Hu–Washizu principle.** Within the enhanced strain formulations, non-conforming strain measures are introduced within the Hu–Washizu principle. In a first paper, Simo and Rifai (1990) developed *enhanced strain* elements for the geometrical linear theory.

   In follow up work, Simo and Armero (1992) and Simo et al. (1993b) have derived a family of enhanced elements for large deformations and inelastic constitutive equations based in the Hu–Washizu. This class of elements is related to the incompatible mode elements which were developed by Wilson et al. (1973) and Taylor et al. (1976) for linear problems. The *enhanced strain* elements fulfil point 1 to 6 of the above mentioned requirements. Hence they are well suited for all applications. However, these elements have some disadvantageous. They need a statical condensation on element level. For the two-dimensional case, this leads to the inversion of a 4×4 matrix and, depending on the formulation, in the three-dimensional case a 9×9 or 12×12 matrix has to be inverted. This reduces the efficiency of the enhanced strain elements. Furthermore, storage of the degrees of freedom belonging to the enhanced strains needs additional storage on element level, see also the comments regarding Table 10.1. However, a special efficient formulation has been developed in Puso (2000). A further point which is still under investigation is related to the *hour-glassing* of the enhanced strain elements under pressure. This fact was discovered by Wriggers and Reese (1994), see also Wriggers and Reese (1996). A detailed discussion of this phenomenon can

be found in Sect. 10.5. Solutions which partly solve this problem are provided in Korelc and Wriggers (1996a), Glaser and Armero (1997), Reese and Wriggers (2000), Reese (2005) and Mueller-Hoeppe et al. (2008), where different methods have been used to overcome the *hour glassing*, see also Sect. 10.5.4.

It is not possible to enhanced triangular and tetrahedral elements directly. The method is degenerate for triangular and tetrahedral elments, see Reddy and Simo (1995). However, a mixed enhanced approach where ansatz functions for displacements pressures and volume effects are introduced can be employed to generate low order tetrahedral elements which do not lock in incompressibility and perform reasonably well in bending, see e.g. Taylor (1985) and Mahnken et al. (2008).

4. **Mixed variational principles for problems with rotational degrees of freedom.** When not only the momentum is weakly enforced, but also the moment of momentum, which usually leads, see (3.68), to the symmetry of the stress tensor, then rotational degrees of freedom can be introduced as independent field variables. Finite elements which is based on such formulation were constructed in e.g. Hughes and Brezzi (1989). Further applications of such variational formulations can be found for two-dimensional elements which are a basis for shell formulations, see e.g. Ibrahimbegovic et al. (1990), Iura and Atluri (1992) and Gruttmann et al. (1992). A three-dimensional technique using co-rotational formulations for three-dimensional continua was developed in Moita and Crisfield (1996).
5. **Mixed variational principles for special quantities.** Often problems have to be considered which include special constraint conditions. In such cases, it is advantageous to formulate mixed principles which are tailored to fulfil such constraint conditions. Examples are solid elements for plates or shells where, for thin structures, the transverse shear becomes zero in the limit, see also Chap. 9.4. Another example is related to contact problems where the zero gap condition introduces a constraint which has to be considered when deriving associated finite element discretizations, see Chap. 11. The example standing out in solid mechanics is the constraint related to incompressibility. This constraint occurs in rubber elasticity and in case of plastic flow, when the J_2 is applied for mechanical modelling. The related special variational principle relies on a split of the kinematical variables into volumetric and deviatoric parts, details are provided in Sect. 10.2.

   The related finite elements fulfil point 1, 4, 5 and 7 of the above mentioned requirements. Due to the kinematical split, the formulation of the constitutive equations is more elaborate than in the standard

formulation. This is especially true for large deformations making the linearizations, needed within the NEWTON method, more complex.

6. **Nodally based elements.** Nodally based elements are applied to enhance the bending behaviour of tetrahedral elements and to avoid locking in such cases. Besides a number of other formulations, average nodal pressures or strains can be used to compute average volumetric strains or strains at nodes based on surrounding triangles or tetrahedrals, see Dohrmann et al. (2000) and Bonet and Burton (1998). These types of element have been stabilized by Puso and Solberg (2006) in order to alleviate spurious modes.
7. **Composite or macro elements.** Composite or macro element formulations make use of the possibility to construct finite elements from subelements which use simplified or special shape functions. These type of elements can be developed for triangular and quadrilateral shaped elements. For triangles, this type of formulation is, as well as the nodally based formulation, one of the few possibilities to enhance the element behaviour, see Guo et al. (2000) and Thoutireddy et al. (2002), since triangles cannot be enhanced in the standard way using the HU-WASHIZU principle. This technique is not often employed for quadrilaterals and hexahedral elements since the only gain is a more robust behaviour when the elements are distorted severely at large strain states. Here formulations were developed by Rubin and Jabareen (submitted), based on the COSSERAT point theory, and by Boerner and Wriggers (2008) based on the standard continuum approach.
8. **Higher order displacement elements.** During the last years, finite element discretization schemes were developed which is based on higher order interpolation. These methods depict very good convergence characteristics for finite hyperelastic deformations, see e.g. Düster et al. (2003) but also for elasto-plastic problems undergoing small deformations, see Düster et al. (2002). They can be formulated in an efficient way by hierarchical shape functions using polynomials or NURBS and hence are competitive with respect to low order approximations. However, still special techniques have to be employed for incompressible materials in order to recover optimal convergence rates also for lower order approximations, see e.g. Elguedj et al. (2008) and Heisserer et al. (2007).
9. COSSERAT **point elements.** Lately, elements have been formulated which are based on the COSSERAT point theory. This theory formulates the continuum as a point then director vectors are introduced to account for the deformation modes. For a theoretical background, see Rubin (2000). This formulation transforms directly into a finite element discretization, as was shown in Nadler and Rubin (2003). Furthermore, due to an internal split of the deformation modes it is possible to use linear analytical solution to stabilize the element such that *locking* but also *hour glassing* does not occur. The element has so far superior behaviour

problems with hyperelastic materials for undistorted element geometries, fulfilling points 1-5 and 7, but behaves like pure displacement Q1-element for distorted meshes, see Loehnert et al. (2005). For initially distorted element, geometries approaches to improve the element behaviour are discussed in Boerner et al. (2007) and Rubin and Jabareen (2008).

10.2 Mixed Elements for Incompressibility

Pure is displacement elements are not suitable for problems in which the constitutive behaviour exhibit incompressibility since they tend to *locking*. *Locking* means, in this connection, that the constraint conditions due to incompressibility which are related to the pure volumetric mode (in the elastic case the condition is $J = \det \mathbf{F} = 1$ and for plastic flow the condition $J_p = \det \mathbf{F}_p = 1$ holds) can only be fulfilled with a considerable stiffening of the bending modes, see e.g. Hueck et al. (1994). Thus this behaviour is also called volume locking. Mixed finite element methods can help to avoid locking, see e.g. Zienkiewicz and Taylor (1989) and Brezzi and Fortin (1991).
There exist different possibilities to construct mixed elements. These are shortly discussed in the following.

– **Method of** LAGRANGIAN **multipliers.** Here the constraint condition of incompressibility will be directly introduced via the methods of LAGRANGIAN multipliers. Hence the strain energy

$$W = W_{inkomp} + p\,G(J) \quad \text{with} \quad G(J) = 0 \tag{10.1}$$

is formulated. The constraint condition is then given for finite deformations as $G(J) = J - 1$ with $J =$ is e.g. given by the MOONEY–RIVLIN material (3.112). Finite elements which are based on this methodology have the disadvantage that contrary to the pure displacement elements additional unknowns occur. These are the LAGRANGIAN multipliers which are equivalent to the pressure p. Furthermore, special techniques are needed to solve the associated incremental equation system for displacements and LAGRANGIAN multipliers

$$\begin{bmatrix} \boldsymbol{K}_{T\,uu} & \boldsymbol{B}_{T\,up} \\ \boldsymbol{B}_{T\,pu}^T & \boldsymbol{0} \end{bmatrix} \begin{Bmatrix} \Delta \boldsymbol{u} \\ \Delta \boldsymbol{p} \end{Bmatrix} = - \begin{Bmatrix} \boldsymbol{R}_u \\ \boldsymbol{R}_p \end{Bmatrix} \tag{10.2}$$

which has zero entries in the diagonal. The sub-matrix $\boldsymbol{K}_{T\,uu}$ follows from W_{inkomp} while $\boldsymbol{B}_{T\,up}$ is related to the discretization of the term $p\,G(J)$. Associated finite element formulations can be found in Oden and Key (1970) and Duffet and Reddy (1983).

– **Perturbed** LAGRANGIAN **method.** To have a greater variability for the formulation of ansatz functions, the following strain energy function

$$W = W_{inkomp} + p\,G(J) - \frac{1}{2\,\epsilon}\,p^2 \tag{10.3}$$

can be introduced. The constraint condition is again given by $G(J) = J - 1$. $\epsilon > 0$ is a perturbation parameter. Choosing now continuous ansatz function for displacements and pressure, the following incremental equation system can be derived

$$\begin{bmatrix} \boldsymbol{K}_{T\,uu} & \boldsymbol{B}_{T\,up} \\ \boldsymbol{B}_{T\,pu}^{T} & -\frac{1}{\epsilon}\,\boldsymbol{K}_{pp} \end{bmatrix} \left\{ \begin{array}{c} \Delta\boldsymbol{u} \\ \Delta\boldsymbol{p} \end{array} \right\} = - \left\{ \begin{array}{c} \boldsymbol{R}_{u} \\ \boldsymbol{R}_{p\,\epsilon} \end{array} \right\} . \tag{10.4}$$

Here contrary to (10.2), the incremental displacements and pressures can be computed using standard equation solvers. The pressures can be removed from the system by using the SCHUR complement. This leads to

$$\left[\boldsymbol{K}_{T\,uu} + \epsilon\,\boldsymbol{B}_{T\,up}\,\boldsymbol{K}_{pp}^{-1}\,\boldsymbol{B}_{T\,pu}^{T} \right] \Delta\boldsymbol{u} = -\boldsymbol{R}_{u} - \epsilon\,\boldsymbol{B}_{T\,up}\,\boldsymbol{K}_{pp}^{-1}\,\boldsymbol{R}_{p,\epsilon}\,. \tag{10.5}$$

When discontinuous ansatz functions are used for the pressure variables then the pressures can be eliminated on element level. This yields an equation in which the inverse of $\boldsymbol{K}_{pp}$ is trivial

$$\left[\boldsymbol{K}_{T\,uu} + \epsilon\,\boldsymbol{B}_{T\,up}\,\boldsymbol{B}_{T\,pu}^{T} \right] \Delta\boldsymbol{u} = -\boldsymbol{R}_{u} - \epsilon\,\boldsymbol{B}_{T\,up}\,\boldsymbol{R}_{p,\epsilon}\,. \tag{10.6}$$

This system of incremental equations is equivalent to a *penalty* formulation for the incompressibility constraint. Note that the solution now depends on the perturbation or penalty parameter. For small values of ϵ, the influence of the constraint condition disappears. For large values of ϵ, the constraint is fulfilled more and more exactly but the condition number of the linear equation system (10.6) will be very large. Then special equation solvers have to be applied. Papers regarding formulation (10.5) have been published for the linear case by Malkus and Hughes (1978) and for the large strain case of rubber elasticity by e.g. Häggblad and Sundberg (1983) and Sussman and Bathe (1987).

– HU–WASHIZU **functional.** In this functional, the incompressibility constraint is introduced as in the penalty method but is formulated via a constitutive equations for the pressure. In that case the functional

$$H(\boldsymbol{\varphi}\,, p\,, \theta\,) = W(\widehat{\mathbf{C}}) + K\,[\,G(\theta)]^{2} + p\,(J - \theta) \tag{10.7}$$

is formulated, see also Sect. 3.4.3. Within the finite element discretization, ansatz functions are selected for the deformation $\boldsymbol{\varphi}$, the pressure p and the volumetric strain θ. $G(\theta)$ defines the constitutive equation for the pressure term, here K is the modulus of compression. The formulation of $W(\widehat{\mathbf{C}})$ is provided by (3.122). The associated discretization within the finite element method was firstly presented in Simo et al. (1985a).

Finite elements which are derived form mixed methods have to fulfil additional mathematical conditions which guarantee the stability of the element formulation. This condition is known as BB-condition, named after its inventors BABUSKA and BREZZI. Its fulfillment is related to the condition that matrix $\boldsymbol{B}_{T\,pu}$ in (10.4) is not rank deficient.

Remark 10.1: With respect to the mathematical formalism, the BB-condition will be stated here for incompressible linear elasticity. With the short hand notation, see also Chap. 8 and Eq. (8.3), the incompressible problem cab be stated for mixed interpolations as

$$\begin{aligned} a(\mathbf{u}\,,\boldsymbol{\eta}) + b(p\,,\boldsymbol{\eta}) &= f(\boldsymbol{\eta}) \qquad \forall \boldsymbol{\eta} \in V \\ b(q\,,\mathbf{u}) &= 0 \qquad \forall q \in Q \end{aligned} \tag{10.8}$$

where the different terms are given by

$$\begin{aligned} a(\mathbf{u},\boldsymbol{\eta}) &= 2\,\mu \int\limits_{\Omega} \mathbf{e}_D(\boldsymbol{\eta}) \cdot \mathbf{e}_d(\mathbf{u})\, d\Omega\,, \\ b(p\,,\boldsymbol{\eta}) &= \int\limits_{\Omega} p\,\mathrm{div}\,\boldsymbol{\eta}\, d\Omega\,, \\ f(\boldsymbol{\eta}) &= \int\limits_{\Omega} \hat{\mathbf{b}} \cdot \boldsymbol{\eta}\, d\Omega + \int\limits_{\Gamma_\sigma} \hat{\mathbf{t}} \cdot \boldsymbol{\eta}\, d\Gamma\,. \end{aligned} \tag{10.9}$$

The strain deviator $\mathbf{e}_d(\mathbf{u})$, see (3.30), has to be applied in $(10.9)_1$ on order to obtain a clear split between the volumetric strains div$\mathbf{u}$ and the deviatoric part. The incompressibility condition is described by $\mathrm{div}\,\mathbf{u} = 0$ in the linear case. It is introduced to the mixed form by the LAGRANGIAN multiplier method.

In the continuous case of solids with sufficiently smooth boundaries, the displacements are in the SOBOLEV space H^1 ($\mathbf{v} \in V = H^1(\Omega)$, for a definition of the spaces see e.g. (8.7)). For the pressure interpolation, the space L^2 ($p \in Q = L^2(\Omega)$) is sufficient since no derivatives of the pressure variable occur in (10.9). With the finite element ansatz functions for the displacements $\mathbf{u}_h \in V_h \subset V$ and for the pressure $p_h \in Q_h \subset Q$, the discretized form of (10.8) follows

$$\begin{aligned} a(\mathbf{u}_h\,,\boldsymbol{\eta}_h) + b(p_h\,,\boldsymbol{\eta}_h) &= f(\boldsymbol{\eta}_h) \qquad \forall \boldsymbol{\eta}_h \in V_h \\ b(q_h\,,\mathbf{u}_h) &= 0 \qquad \forall q_h \in Q_h. \end{aligned} \tag{10.10}$$

The conditions for existence, uniqueness and stability of the solution are the ellipticity condition and the BB-condition. The first one requires that the ansatz functions $\boldsymbol{\eta}_h$ fulfil for a positive constant $\alpha > 0$, the condition

$$a(\boldsymbol{\eta}_h\,,\boldsymbol{\eta}_h) \geq \alpha \,\|\,\boldsymbol{\eta}_h\,\|_V^2\,. \tag{10.11}$$

The fulfillment of the BB-condition means that a constant $\beta > 0$ exists so that

$$\inf_{q_h \in Q_h} \sup_{\eta_h \in V_h} \frac{b(\,\boldsymbol{\eta}_h\,,q_h\,)}{\|\,\boldsymbol{\eta}_h\,\|_{H^1}\,\|\,q_h\,\|_{L^2}} \geq \beta\,. \tag{10.12}$$

In case that the ansatz functions fulfil both conditions for incompressible material then the derived finite element method is stable.

For general nonlinear applications, there exists no formulation of the BB-condition. One can apply the condition analogously for the tangent spaces which belong to a given state of deformation and pressure, as e.g. provided in (10.2). The BB-condition has the disadvantage that it cannot be formulated for e single element. One always has to consider a patch of elements, see e.g. B Brezzi and Fortin (1991) or Braess (2007). A numerical method to show fulfillment of the BB-condition was derived in Chapelle and Bathe (1993).

10.2.1 Mixed Q1-P0 Element

In this section, a large deformation finite element is derived which is based on the Hu–Washizu variational formulation. This element is implemented in many existing finite element codes and uses linear shape functions for the deformation field related to the deviatoric kinematical variables. Additionally, constant ansatz functions are applied to discretize the pressure and volumetric strain.

The continuum mechanical basis for the mixed Q1-P0 element was already discussed in Sect. 3.4.3. Equation (3.308) describes the weak form with respect to the spatial configuration. Inserting the finite element approximation into the weak form yields with (4.94)

$$\nabla^S \boldsymbol{\eta}_e = \sum_{I=1}^{n} \boldsymbol{B}_{0\,I}\, \boldsymbol{\eta}_I \,. \tag{10.13}$$

The virtual strain $\operatorname{div} \boldsymbol{\eta}$, related to the change of volume, occurs additionally in (3.308). Discretization of the divergence operator leads to

$$\operatorname{div} \boldsymbol{\eta}_e = \sum_{I=1}^{n} \boldsymbol{B}_{V\,I}\, \boldsymbol{\eta}_I \,, \tag{10.14}$$

where the matrix

$$\boldsymbol{B}_{V\,I} = < N_{I\,,1}\,, N_{I\,,2}\,, N_{I\,,3} > \tag{10.15}$$

was introduced. The derivatives have to be computed with respect to the current coordinates, as shown in Sect. 4.2.3.

Furthermore, constant ansatz functions are introduced for the pressure $J\,p = \tau_{vol}$, see (3.129), and the volume strain θ_e in Ω_e

$$\tau_{vol\,e} = J\,p_e = J\,\bar{p} \qquad \theta_e = \bar{\theta}\,. \tag{10.16}$$

With these interpolations, the weak form (3.308) can be written as

$$D\Pi(\boldsymbol{\varphi}, p, \theta) \cdot \boldsymbol{\eta} \;=\; \bigcup_{e=1}^{n_e} \sum_{I=1}^{n} \boldsymbol{\eta}_I^T \int_{\Omega_e} \{\, (\, \boldsymbol{B}_{0\,I}^T\, \boldsymbol{\tau}_{iso\,e} + J\, \boldsymbol{B}_{V\,I}^T\, \bar{p}\,\}\, d\Omega - \delta P_{EXT} = 0,$$

$$
\begin{aligned}
D\Pi(\boldsymbol{\varphi}, p, \theta)\,\delta p &= \int_{\Omega_e} \delta\bar{p}\,(\,J_e - \bar{\theta}\,)\,d\Omega = 0, \qquad (10.17)\\
D\Pi(\boldsymbol{\varphi}, p, \theta)\,\delta\theta &= \int_{\Omega_e} \delta\bar{\theta}\,\left(\frac{\partial W}{\partial\theta} - \bar{p}\right)\,d\Omega = 0\,.
\end{aligned}
$$

The integrals are evaluated with respect to the initial configuration. The first equation denotes the weak form of equilibrium where $\boldsymbol{\tau}$ are the KIRCHHOFF stresses. The second equation is associated with the constraint equation $J_e = \bar{\theta}$ and the third equation yields the constitutive equation for the pressure $\bar{p}$, see also $(3.130)_1$. The last two equations in (10.17) can be fulfilled locally on element level since a discontinuous ansatz was selected for pressure and volume strain. Hence both equations can be solved directly. This leads with (3.12) to

$$
\begin{aligned}
\bar{\theta} &= \frac{1}{\Omega_e}\int_{\Omega_e} J_e\,d\Omega = \frac{\varphi(\Omega_e)}{\Omega_e}\\
\bar{p} &= \frac{1}{\Omega_e}\int_{\Omega_e} \frac{\partial W}{\partial\theta}\,d\Omega = \frac{\partial W}{\partial\theta}(\bar{\theta}) \qquad (10.18)
\end{aligned}
$$

The discretization of the weak form (3.308) is now completed and summarized in Eq. $(10.17)_1$ and (10.18). Note that the volumetric variable θ follows simply from the ratio of the element volume in the current configuration $\varphi(\Omega_e)$ to the element volume in the initial configuration Ω_e.

10.2.2 Linearization of the Q1-P0 Element

The linearization of (10.17) yields a matrix form of the Q1-P0 element in which all variables $(\,\boldsymbol{\varphi}\,, p\,, \theta\,)$ are present. From the first equation of (10.17), the linearization follows with (3.277), (4.112) and (4.113) as

$$
D^2\Pi\cdot\Delta u = \bigcup_{e=1}^{n_e}\sum_{I=1}^{n}\boldsymbol{\eta}_I^T[\sum_{K=1}^{n}\bar{\boldsymbol{K}}^u_{T_{IK}}\Delta\boldsymbol{u}_K + \bar{\boldsymbol{K}}^p_{T_I}\Delta\bar{p}] \qquad (10.19)
$$

where the matrices

$$
\begin{aligned}
\bar{\boldsymbol{K}}^u_{T_{IK}} &= \int_{\Omega_e}\big[\,(\nabla_{\bar{x}}N_I)^T\,(\,\bar{p}\,J\,\mathbf{1} + \bar{\boldsymbol{\tau}}_{iso\,e}\,)\,\nabla_{\bar{x}}N_K\\
&\quad +.\bar{\boldsymbol{B}}^T_{0\,I}\,\big[(\,\mathbf{1}\otimes\mathbf{1} - 2\mathbb{E}\,)\,\bar{p}\,J + \mathfrak{c}_{iso}\,\big]\,\bar{\boldsymbol{B}}_{0\,K}\,\big]\,d\Omega\,, \qquad (10.20)\\
\bar{\boldsymbol{K}}^p_{T_I} &= \int_{\Omega_e}\boldsymbol{B}^T_{V\,I}\,J\,d\Omega\,.
\end{aligned}
$$

occur. The linearization of the second equation (10.17) is derived with the JACOBI determinant, see (3.330), and its associated discretization, see (10.14),

$$\Delta\theta = \frac{1}{\Omega_e} \sum_{K=1}^{n} \int_{\Omega_e} \boldsymbol{B}_{V\,K}\, J\, d\Omega\, \Delta \boldsymbol{u}_K\,. \tag{10.21}$$

The third equation of (10.17) yields the linearization

$$\Delta\bar{p} = \frac{\partial^2 W}{\partial \theta^2}\Delta\theta\,. \tag{10.22}$$

Inserting now (10.21) in (10.22) and using this result in (10.19) and (10.20) leads to the elimination of the variables for pressure $\Delta\bar{p}$ and volumetric strain $\Delta\theta$ on element level. Thus a pure displacement formulation is obtained. Its tangent stiffness matrix has, for the element nodes I and K, the following expression

$$\begin{aligned} \bar{\boldsymbol{K}}^{Q1P0}_{T_{IK}} \;=\; & \int_{\Omega_e} \big[\, (\nabla_{\bar{x}} N_I)^T \,(\,\bar{p}\, J\, \mathbf{1} + \bar{\boldsymbol{\tau}}_{iso\,e}\,)\, \nabla_{\bar{x}} N_K \\ & +.\bar{\boldsymbol{B}}^T_{0\,I}\, \big[(\,\mathbf{1}\otimes\mathbf{1} - 2\mathbb{E}\,)\,\bar{p}\, J + \mathfrak{C}_{iso}\,\big]\,\bar{\boldsymbol{B}}_{0\,K}\,\big]\; d\Omega \\ & +\frac{1}{\Omega_e}\int_{\Omega_e} \boldsymbol{B}^T_{V\,I}\, J\, d\Omega \left(\frac{\partial^2 W}{\partial\theta^2}\,\Omega_e\right) \frac{1}{\Omega_e}\int_{\Omega_e} \boldsymbol{B}_{V\,K}\, J\, d\Omega\,. \end{aligned} \tag{10.23}$$

This element does not fulfil the BB-condition in the geometrical linear theory. Thus it can lead to unstable solutions for the pressure when special loading and boundary conditions are given. Often post-processing of the pressures using L^2 smoothing can help. In practical application, it has been observed that this element is quite robust for many problems in solid mechanics which depict quasi-incompressible material behaviour. Hence it is contained in many commercial finite element codes. In case that this element is not sufficient, its high order variant can be used which is the Q2-P1 element with quadratic interpolations for the deformations and linear interpolation for the pressure. It fulfils the BB-condition in case of the linear theory, see e.g. Brezzi and Fortin (1991).

10.3 Mixed Finite Elements for Finite Elasticity

A mixed finite element, based on the Neo–Hooke material equation (3.119) in Sect. 3.3.1, is developed by using a formulation equivalent to the Hellinger–Reissner principle, see e.g. Washizu (1975). The main idea is to use a similar approach as the one advocated by Pian and Sumihara (1984) for the linear case. Within this hybrid approach, the constitutive equation needed to be inverted. Here the Neo–Hooke material equation is given for the 2nd Piola–Kirchhoff stress $\mathbf{S}$ in terms of the right Cauchy–Green tensor $\mathbf{C}$ as

$$\mathbf{S} = \frac{\Lambda}{2}\,(J^2-1)\,\mathbf{C}^{-1} + \mu\,(\,\mathbf{1} - \mathbf{C}^{-1}\,)\,. \tag{10.24}$$

Under the assumption that it is possible to invert this equation form,

$$\mathbf{C} = \mathbf{f}(\mathbf{S}) \tag{10.25}$$

is obtained.

For the derivation of the mixed hybrid principle in Pian and Sumihara (1984), the classical LEGENDRE transformation $\frac{1}{2}\boldsymbol{\epsilon}\cdot\mathbb{C}[\boldsymbol{\epsilon}] = \boldsymbol{\sigma}\cdot\boldsymbol{\epsilon} - \frac{1}{2}\boldsymbol{\sigma}\cdot\mathbb{C}^{-1}[\boldsymbol{\sigma}]$ was applied. This transformation, a however, a is not valid in the nonlinear case, see e.g. Ogden (1984) and hence cannot be applied the Neo–HOOKE material. Instead, a weak form of the equilibrium G_u and the constitutive relation G_c is formulated which has as primary variables the displacement field and the stress field as follows

$$\begin{aligned} G_u(\mathbf{u}\,,\mathbf{S}\,,\boldsymbol{\eta}) &= \int\limits_B \frac{1}{2}\,\mathbf{S}\cdot\mathbf{C}(\boldsymbol{\eta})\,dV - \int\limits_B \hat{\mathbf{b}}\cdot\boldsymbol{\eta}\,dV - \int\limits_{\partial B_\sigma} \hat{\mathbf{t}}\cdot\boldsymbol{\eta}\,dA = 0\,, \\ G_c(\mathbf{u}\,,\mathbf{S}\,,\mathbf{Q}) &= \int\limits_B \frac{1}{2}\,\mathbf{Q}\cdot[\,\mathbf{C}(\mathbf{u}) - \mathbf{f}(\mathbf{S})\,]\,dA = 0\,. \end{aligned} \tag{10.26}$$

Here $\boldsymbol{\eta}$ and $\mathbf{Q}$ are the test functions, $\boldsymbol{\eta}$ is equivalent to the virtual displacement and $\mathbf{Q}$ to the virtual stress. $\mathbf{C}(\boldsymbol{\eta}) = \mathbf{F}^T\,\mathrm{Grad}\,\boldsymbol{\eta} + \mathrm{Grad}^T\,\boldsymbol{\eta}\,\mathbf{F}$ is the virtual strain and $\mathbf{C}(\mathbf{u}) = \mathbf{F}^T\,\mathbf{F}$ is the right CAUCHY–GREEN tensor; the latter depending only on the displacement field $\mathbf{u}$. This weak form can be viewed as the nonlinear version of the HELLINGER–REISSNER functional.

Note that the inverse (10.25) is not uniquely defined, either locally or globally, see Ogden (1984). However, (10.24) can be inverted by looking at different solution branches. For this (10.24) is rewritten as

$$\hat{\mathbf{A}}(\mathbf{S}) = \hat{\beta}(\mathbf{C})\,\mathbf{C}^{-1} \tag{10.27}$$

with

$$\begin{aligned} \hat{\beta} &= \alpha - J^2, \\ \alpha &= 1 + \frac{2\mu}{\Lambda}, \\ \hat{\mathbf{A}}(\mathbf{S}) &= \frac{2}{\Lambda}\,(\,\mu\mathbf{1} - \mathbf{S}\,). \end{aligned} \tag{10.28}$$

Multiplication of (10.27) with $\hat{\mathbf{A}}^{-1}$ from the left side leads to

$$\mathbf{C} = \hat{\beta}(\mathbf{C})\,\hat{\mathbf{A}}^{-1}(\mathbf{S})\,. \tag{10.29}$$

Now it remains to compute $\hat{\beta}(\mathbf{C})$ in dependence of $\hat{\mathbf{A}}$. The computation of the determinant of (10.29) yields

$$\det \hat{\mathbf{A}} = \frac{\hat{\beta}^3}{J^2} \tag{10.30}$$

since $J^2 = \det \mathbf{C}$. With the abbreviation $\hat{a} = \det \hat{\mathbf{A}}$ and $(10.28)_1$ this leads to a cubic equation for $\hat{\beta}$:

$$\hat{\beta}^3 + \hat{\alpha}\,\hat{\beta} - \hat{a}\alpha = 0\,. \tag{10.31}$$

To obtain a simpler solution $\beta = c_1\,\hat{\beta}$, $\mathbf{A} = c_2\,\hat{\mathbf{A}}$ and $a = \det \mathbf{A}$ can be defined. Together with c_1 and c_2

$$c_1 = \frac{2}{3\,\alpha}\,, \qquad c_2 = \frac{1}{3}\left[\frac{4}{\alpha^2}\right]^{\frac{1}{3}}\,, \tag{10.32}$$

which only depend on the LAME constants, this provides the cubic equation for β

$$\beta^3 + 3\,a\,\beta - 2\,a = 0\,. \tag{10.33}$$

Depending on the discriminant $D = a^3 + a^2$, three different solutions have to be distinguished:

– $D > 0$: Equation (10.33) has only one real solution

$$\beta = r - \frac{a}{r} \qquad \text{with} \quad r = \left[a + \sqrt{a^3 + a^2}\right]^{\frac{1}{3}}\,. \tag{10.34}$$

– $D < 0$: This case is equivalent to $a < -1$ and yields three solutions for (10.33)

$$\beta = -2\sqrt{-a}\,\cos\left[\frac{1}{3}\,(\,\arccos\frac{1}{\sqrt{-a}} + 2\,\pi\,k\,)\right]\,, \qquad k = 0\,,1\,,2. \tag{10.35}$$

In the physical problem, $J > 0$ has to be fulfilled. From $(10.28)_1$ and $(10.32)_1$ it then follows that $\beta < \frac{2}{3}$. Hence only the solution with $k = 0$ remains under these circumstances

$$\beta = -2\sqrt{-a}\,\cos\left(\frac{1}{3}\,\arccos\frac{1}{\sqrt{-a}}\right). \tag{10.36}$$

– $D = 0$: Here the determinant a is either $a = 0$ or $a = -1$. For $a = 0$, the only solution is $\beta = 0$ which yields with $(10.28)_1$ and $(10.32)_1$ for the JACOBIAN $J = \sqrt{\alpha}$. For $a = -1$, β can be obtained from (10.36), leading in the limit to $\beta = -2$.

Based on this solution, the expression for the inverse of the Neo–HOOKE material (10.24) can be derived, by employing $(10.28)_1$ and $(10.28)_3$. With

$$\mathbf{A} = \frac{2}{3\,\Lambda}\,\left[\frac{4}{\alpha^2}\right]^{\frac{1}{3}}\,(\,\mu\mathbf{1} - \mathbf{S}\,), \tag{10.37}$$

the final result is obtained

$$\mathbf{C} = \beta \left[\frac{\alpha}{2}\right]^{\frac{1}{3}} \mathbf{A}^{-1} = \frac{3}{4}\beta\,\alpha\,\Lambda\,(\,\mu\mathbf{1} - \mathbf{S}\,)^{-1}\,. \tag{10.38}$$

Hence it is possible to invert the constitutive equation; the weak formulation (10.26) related to a HELLINGER–REISSNER functional can be used as starting point for the finite element development.

Interpolation has to be selected for the displacement field and the stresses. Here a four-node quadrilateral is derived based on the isoparametric concept. For the displacement field and its variation, the standard shape functions are used

$$\mathbf{u} = \sum_{I=1}^{4} N_I(\xi\,,\eta)\,\mathbf{u}_I\,, \qquad \boldsymbol{\eta} = \sum_{I=1}^{4} N_I(\xi\,,\eta)\,\boldsymbol{\eta}_I. \tag{10.39}$$

As usual, the coordinates are expressed by the same approximation

$$\mathbf{X} = \sum_{I=1}^{4} N_I(\xi\,,\eta)\,\mathbf{X}_I, \tag{10.40}$$

where the nodal coordinates $\boldsymbol{X}_I$ are related to the initial configuration and ξ, η are convective coordinates with regard to the reference element. The interpolation function is given by, see Sect. 4.1.2,

$$N_I = \frac{1}{4}\,(\,1 + \xi\,\xi_I\,)\,(\,1 + \eta\,\eta_I\,)\,. \tag{10.41}$$

The interpolation introduced by Pian and Sumihara (1984) is chosen for the stress field. It leads to the matrix form

$$\left\{\begin{array}{c} S^{\xi\,\xi} \\ S^{\eta\eta} \\ S^{\xi\eta} \end{array}\right\} = \begin{bmatrix} 1 & 0 & 0 & \eta & 0 \\ 0 & 1 & 0 & 0 & \xi \\ 0 & 0 & 1 & 0 & 0 \end{bmatrix} \left\{\begin{array}{c} \bar{s}_1 \\ \bar{s}_2 \\ \bar{s}_3 \\ \bar{s}_4 \\ \bar{s}_5 \end{array}\right\} \tag{10.42}$$

with respect to the reference element. Note that the stress components are usually contravariant which is in accordance with the stress power $S^{ik}\,\dot{C}_{ik}$ and the definition of the strain measures via the deformation gradient.

The stresses in the reference element ($\mathbf{S} = S^{\alpha\beta}\,\mathbf{G}_\alpha \otimes \mathbf{G}_\beta$) have now to be transformed to the global coordinate system which is obtained by

$$\begin{aligned} S^{ik} &= \mathbf{E}^i \cdot \mathbf{S}\,\mathbf{E}^k = \mathbf{E}_i \cdot (\,S^{\alpha\beta}\,\mathbf{G}_\alpha \otimes \mathbf{G}_\beta\,)\,\mathbf{E}_k \\ &= S^{\alpha\beta}(\mathbf{E}_i \cdot \mathbf{G}_\alpha)(\mathbf{E}_k \cdot \mathbf{G}_\beta). \end{aligned}$$

For the orthogonal basis, the relation $\mathbf{E}^i = \mathbf{E}_i$ holds. Furthermore, a matrix form of this transformation can be defined which is given by $\mathbf{S}(\mathbf{X}) = \mathbf{T}\,\mathbf{S}(\boldsymbol{\xi})\,\mathbf{T}^T$. In detail

$$\begin{bmatrix} S^{xx} & S^{xy} \\ S^{yx} & S^{yy} \end{bmatrix} = \begin{bmatrix} T_{11} & T_{12} \\ T_{21} & T_{22} \end{bmatrix} \begin{bmatrix} S^{\xi\xi} & S^{\xi\eta} \\ S^{\eta\xi} & S^{\eta\eta} \end{bmatrix} \begin{bmatrix} T_{11} & T_{21} \\ T_{12} & T_{22} \end{bmatrix} \tag{10.43}$$

is derived, where $T_{i\alpha} = \mathbf{E}_i \cdot \mathbf{G}_\alpha$.

The base vectors can be computed from the isoparametric interpolation since $\mathbf{G}_\alpha = \mathbf{X}_{,\alpha}$

$$\mathbf{G}_\alpha = \sum_{I=1}^{4} N_I(\xi\,,\eta)_{,\alpha}\,\mathbf{X}_I\,. \tag{10.44}$$

Hence

$$T_{i\alpha} = \sum_{I=1}^{4} N_I(\xi\,,\eta)_{,\alpha}\,X_{i\,I}, \tag{10.45}$$

where $X_{i\,I} = \mathbf{E}_i \cdot \mathbf{X}_I$. Using the interpolation (10.41), the derivatives are

$$N_{I\,,\xi} = \frac{\xi_I}{4}\,(\,1 + \eta\,\eta_I\,), \qquad N_{I\,,\eta} = \frac{\eta_I}{4}\,(\,1 + \xi\,\xi_I\,)\,. \tag{10.46}$$

The transformation matrix will be evaluated at the element centre $\xi = \eta = 0$ leading to

$$N^0_{I\,,\xi} = \frac{\xi_I}{4}, \qquad N^0_{I\,,\eta} = \frac{\eta_I}{4}\,. \tag{10.47}$$

and

$$T^0_{i\xi} = \sum_{I=1}^{4} \frac{\xi_I}{4}\,X_{i\,I} \quad \text{and} \quad T^0_{i\eta} = \sum_{I=1}^{4} \frac{\eta_I}{4}\,X_{i\,I}\,. \tag{10.48}$$

Due to this, the transformation matrix is given by

$$\mathbf{T}^0 = \frac{1}{4}\sum_{I=1}^{4} \begin{bmatrix} \xi_I\,X_{1\,I} & \eta_I\,X_{1\,I} \\ \xi_I\,X_{2\,I} & \eta_I\,X_{2\,I} \end{bmatrix}\,. \tag{10.49}$$

By performing the multiplication in (10.43) and rearranging the components of the stress tensor in VOIGT notation, the stress transformation can be written as

$$\begin{Bmatrix} S^{xx} \\ S^{yy} \\ S^{xy} \end{Bmatrix} = \begin{bmatrix} T^2_{11} & T^2_{12} & 2\,T_{11}\,T_{12} \\ T^2_{21} & T^2_{22} & 2\,T_{21}\,T_{22} \\ T_{11}\,T_{21} & T_{22}\,T_{12} & T_{12}\,T_{21} + T_{11}\,T_{22} \end{bmatrix} \begin{Bmatrix} S^{\xi\xi} \\ S^{\eta\eta} \\ S^{\xi\eta} \end{Bmatrix}\,. \tag{10.50}$$

Since the stress interpolation (10.42) is constant for the shear stresses and the transformation matrix is constant element wise, a different representation can be found using the element wise constant matrix $\mathbf{s}^T = \{\,s_1\,,s_2\,,s_3\,,s_4\,,s_5\,\}$. This ansatz can be written in global coordinates using the transformation (10.50) at the mid point of the element and leads to the simpler form

$$\begin{Bmatrix} S^{xx} \\ S^{yy} \\ S^{xy} \end{Bmatrix} = \begin{Bmatrix} s_1 \\ s_2 \\ s_3 \end{Bmatrix} + \begin{bmatrix} \eta\,(T^0_{11})^2 & \xi\,(T^0_{12})^2 \\ \eta\,(T^0_{21})^2 & \xi\,(T^0_{22})^2 \\ \eta\,T^0_{11}\,T^0_{21} & \xi\,T^0_{22}\,T^0_{12} \end{bmatrix} \begin{Bmatrix} s_4 \\ s_5 \end{Bmatrix}\,. \tag{10.51}$$

These interpolations can now be used within the mixed weak form (10.26) and its linearization to derive the matrix form of the associated finite element formulation.

10.4 Stabilized Finite Elements

Stabilized finite elements are formulated in order to obtain efficient elements for which the residual vector and tangent matrix can be computed in a fast way and which need, as few as possible, memory to store history variables related to the chosen constitutive equations. The simplest method to achieve these two goals is to apply reduced integration which is based on a minimum number of GAUSS points and hence has less computational effort and storage requirement for history data. The drawback is that these elements are generally unstable since reduced integration is associated with rank deficiency. Thus underintegrated elements have to be stabilized. Stabilization is performed based on the eigenmodes of the elements. These follow from an eigenvalue analysis of a single finite element matrix. Here zero eigenvalues occur for rigid body modes which naturally do not contribute to the element stiffness. Additional zero eigenvalues have to be stabilized and hence an artificial stiffness has to be introduced to prevent non-physical occurrence of these modes within a finite element analysis.

For the two-dimensional linear elastic case, the eigenvectors computed from the spectral decomposition of the stiffness matrix are depicted in Fig. 10.1, excluding the rigid body modes. The eigenvectors related to the volume change, the elongation and shear can be found in the first row. The second row shows the bending modes of the element. It is well known from the linear theory that the eigenvalues related to the bending modes are zero when reduced integration is applied. In that case, no strain energy is associated with these modes. Hence deformations related to the bending modes can occur in an analysis depending on the loading and boundary conditions. Since two of the bending modes can form an *hour-glass*, these modes are also called *hour-glass* modes, see Fig. 10.2b.

Thus stabilization has to be used to avoid hour-glassing when underintegrated elements are applied within a finite element analysis. In this case,

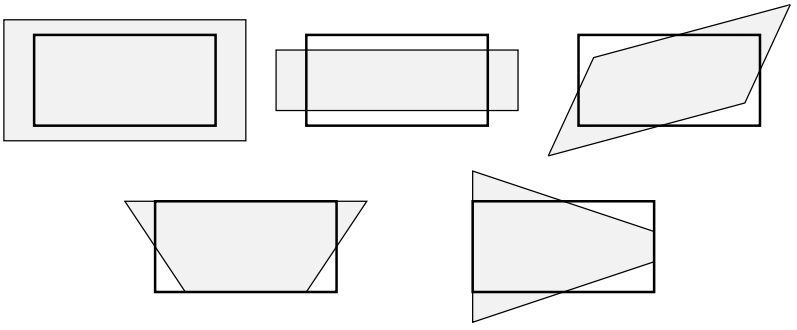

Fig. 10.1 Eigenvectors of the quadrilateral 4-node element

the eigenvectors related to hour-glassing are determined in the initial configuration and then stabilized. This procedure is however not trivial: the mode of a distorted element has to be determined and the magnitude of the stiffness to be added cannot be derived directly from the underlying variational equation.

Two basic approaches are possible.

1. Hour-glass modes can be filtered from the global solution as discussed in Jaquotte and Oden (1986). This however is only possible for elastic problems.
2. The displacement interpolation can be decomposed within a finite element into an linear part and the related orthogonal part. The latter is then used to derive a stabilization matrix. This idea was developed in Kosloff and Frazier (1978) for linear problems. A follow up paper from Belytschko et al. (1984), see also Hughes (1987, p. 251), introduces the so-called $\boldsymbol{\gamma}$ vectors. Their explicit form can be used to construct the stabilization matrix.

While it is possible to compute the stiffness parameters for the stabilization matrix from the equivalence of mixed methods and stabilized reduced integration procedures, see e.g. the element formulation developed in Pian and Sumihara (1984), this has so far not been achieved for nonlinear problems in a satisfactory way. Approaches can be found in Belytschko and Bindeman (1991), Belytschko and Bindeman (1993), Bonet and Bhargava (1995), Reese et al. (1998) and Reese (2005), see also Sect. 10.5.

The classical stabilization procedure for underintegrated element will be developed in the following for three-dimensional hexahedral elements with linear displacement interpolation. Basically, the tangent stiffness matrix (4.76) which was already derived in Sect. 4.2.2 is evaluated by using a one point GAUSS integration instead of the rank preserving $2 \times 2 \times 2$ integration

$$\bar{\boldsymbol{K}}^{1\times 1}_{T_{IK}} = \int_{\Omega_e} \left[(\nabla_X N_I)^T \, \bar{\boldsymbol{S}} \nabla_X N_K + \bar{\boldsymbol{B}}^T_{L\,I} \, \bar{\boldsymbol{D}} \, \bar{\boldsymbol{B}}_{L\,K} \right] d\Omega \,.$$

The matrix form is provided for the nodal combination $I\,, K$ of a finite element Ω_e. Within this notation, the sub matrix $\bar{\boldsymbol{K}}_{T_{IK}}$ has the size $n_{dof} \times n_{dof}$ where n_{dof} is the number of degrees of freedom needed to describe the displacement field (for three-dimensional problems $n_{dof} = 3$ holds). The indices I and K are nodes of the element and directly related to the discretization. Summation over all 8 nodes of the hexahedral element yields the tangent matrix for the finite element e: $\bar{\boldsymbol{K}}^{1\times 1}_{T_e}$. Note that a 1-point-integration requires only one evaluation within the element mid point, see Table 4.1

$$\bar{\boldsymbol{K}}^{1\times 1}_{T_e} = \bar{\boldsymbol{K}}_{T_e}\big|_{\xi=\eta=\zeta=0} \,. \tag{10.52}$$

Hence all terms can be neglected which depend on the coordinates $\xi\,, \eta$ or ζ. This procedure simplifies the coding of such element and thus leads to a high efficiency.

The stabilization matrix $\bar{\boldsymbol{K}}_{T_e}^{stab}$ is added to (10.52) which leads to

$$\bar{\boldsymbol{K}}_{T_e} = \bar{\boldsymbol{K}}_{T_e}^{1\times 1} + \bar{\boldsymbol{K}}_{T_e}^{stab} \tag{10.53}$$

with the diagonalized form, see Belytschko et al. (1984),

$$\bar{\boldsymbol{K}}_{T_e}^{stab} = \sum_{k=1}^{12} \alpha_k \, \bar{\boldsymbol{\gamma}}_k \, \bar{\boldsymbol{\gamma}}_k^T \,. \tag{10.54}$$

The scalar parameters $\alpha_k > 0$ can be chosen arbitrarily. However, their magnitude has to be selected such that the parameters avoid hour-glassing on one side and do not influence the solution of the problem on the other side. This however is not always possible, see examples in Reese (1994). Hence the user of stabilized elements has to have sufficient experience when applying this method.

The determination of the $\bar{\boldsymbol{\gamma}}_k$ vectors for stabilization will be presented in the next section. Kosloff and Frazier (1978) have already shown that the diagonal form of $\bar{\boldsymbol{K}}_{T_e}^{stab}$ using 12 scalar parameters, see (10.54), is not sufficient to obtain optimal bending behaviour for generally distorted three-dimensional meshes. Thus the stabilization matrix in (10.54) yields good results for application which do not exhibit bending.

10.4.1 Stabilization Vectors

The isoparametric ansatz functions presented in Sect. 4.1.3 can also be written in an equivalent vector form. This is advantageous when stabilization vectors have to be derived. Instead of (4.40), the interpolation functions are given by

$$\boldsymbol{N}(\boldsymbol{\xi}) = \frac{1}{8} \left[\, \boldsymbol{a}_1 + \xi \, \boldsymbol{a}_2 + \eta \, \boldsymbol{a}_3 + \zeta \, \boldsymbol{a}_4 + \eta \, \zeta \, \boldsymbol{a}_5 + \xi \, \zeta \, \boldsymbol{a}_6 + \xi \, \eta \, \boldsymbol{a}_7 + \xi \, \eta \, \zeta \, \boldsymbol{a}_8 \, \right] \tag{10.55}$$

with the constant vectors

$$\begin{aligned}
\boldsymbol{a}_1^T &= \{\ 1\,,\ \ 1\,,\ \ 1\,,\ \ 1\,,\ \ 1\,,\ \ 1\,,\ \ 1\,,\ \ 1\,\} \\
\boldsymbol{a}_2^T &= \{-1\,,\ \ 1\,,\ \ 1\,,-1\,,-1\,,\ \ 1\,,\ \ 1\,,-1\,\} \\
\boldsymbol{a}_3^T &= \{-1\,,-1\,,\ \ 1\,,\ \ 1\,,-1\,,-1\,,\ \ 1\,,\ \ 1\,\} \\
\boldsymbol{a}_4^T &= \{-1\,,-1\,,-1\,,-1\,,\ \ 1\,,\ \ 1\,,\ \ 1\,,\ \ 1\,\} \\
\boldsymbol{a}_5^T &= \{\ \ 1\,,\ \ 1\,,-1\,,-1\,,-1\,,-1\,,\ \ 1\,,\ \ 1\,\} \\
\boldsymbol{a}_6^T &= \{\ \ 1\,,-1\,,-1\,,\ \ 1\,,-1\,,\ \ 1\,,\ \ 1\,,-1\,\} \\
\boldsymbol{a}_7^T &= \{\ \ 1\,,-1\,,\ \ 1\,,-1\,,\ \ 1\,,-1\,,\ \ 1\,,-1\,\} \\
\boldsymbol{a}_8^T &= \{-1\,,\ \ 1\,,-1\,,\ \ 1\,,\ \ 1\,,-1\,,\ \ 1\,,-1\,\}\,.
\end{aligned}$$

By using this notation, the interpolation of the components of the displacement vector $\mathbf{u}_e = u_i\,\mathbf{E}_i$ can be written as

$$u_1 = \boldsymbol{N}^T\,\boldsymbol{v}_1\,, \qquad u_2 = \boldsymbol{N}^T\,\boldsymbol{v}_2\,, \qquad u_3 = \boldsymbol{N}^T\,\boldsymbol{v}_3\,, \tag{10.56}$$

where the vectors $\boldsymbol{v}_i$ contain the components of the nodal displacements in coordinate direction i. The stabilization vectors follow from a TAYLOR expansion of the shape functions with respect to the midpoint of the element $\boldsymbol{\xi} = \mathbf{0}$ up to first order terms. This yields for the ansatz functions

$$\boldsymbol{N} = \boldsymbol{N}_0 + \left.\frac{\partial \boldsymbol{N}}{\partial \boldsymbol{X}}\right|_{\boldsymbol{\xi}=\mathbf{0}} (\,\boldsymbol{X} - \boldsymbol{X}_{|\,0}\,) + \boldsymbol{N}_\gamma \tag{10.57}$$

with a constant term $\boldsymbol{N}_0$, a linear term and a residual term $\boldsymbol{N}_\gamma$. $\boldsymbol{X}_0$ is the position vector of the element midpoint. Since it is not possible to differentiate in (10.57) with respect to $\boldsymbol{X}$, the chain rule and thus the JACOBI matrix $\boldsymbol{J}_e$ has to be used, see Sect. 4.1, to obtain

$$\begin{aligned} \boldsymbol{N} &= \boldsymbol{N}_0 + \left(\frac{\partial \boldsymbol{N}}{\partial \boldsymbol{\xi}}\,\boldsymbol{J}_e^{-1}\right)\Big|_{\boldsymbol{\xi}=\mathbf{0}} (\,\boldsymbol{X} - \boldsymbol{X}_{|\,0}\,) + \boldsymbol{N}_\gamma \\ &= [\,\boldsymbol{I} - (\boldsymbol{N}_{,\xi}\,\boldsymbol{J}_e^{-1}\,)_{|\,0}\,\boldsymbol{X}_{kn}\,]\frac{1}{8}\,\boldsymbol{a}_1 + (\boldsymbol{N}_{,\xi}\,\boldsymbol{J}_e^{-1}\,)_{|\,0}\,\boldsymbol{X} + \boldsymbol{N}_\gamma\,. \end{aligned} \tag{10.58}$$

The matrix $\boldsymbol{X}_{kn}$ of dimension 3×8 was introduced for a more compact notation. It contains the coordinates $\{\,X_I\,, Y_I\,, Z_I\,\}$ of the position vectors to the element nodes $I = 1, 8$. The index 0 at $\boldsymbol{J}_{|\,0}$ means that $\boldsymbol{J}_e$ has to be evaluated at $\boldsymbol{\xi} = \mathbf{0}$. The first two terms in (10.58) represent a vector of the shape functions which is linear in $\boldsymbol{X}$. Note that this relation is valid for arbitrarily deformed element geometries in the initial configuration. The residual term can now be determined from $\boldsymbol{N}_\gamma = \boldsymbol{N} - \boldsymbol{N}_{lin}$. Within this procedure, the convergence criteria for finite elements have to be fulfilled, see the preliminary remarks in Sect. 8. For this rigid body modes and constant strains have to be recovered for arbitrary element geometries. This requires that vector $\boldsymbol{N}_\gamma$ has to be orthogonal to the linear part of the shape functions; otherwise it is impossible to obtain constant strain states. This is associated with the classical requirement of the fulfillment of the *patch tests*, see e.g. Bathe (1982) and Hughes (1987). By considering the aforementioned orthogonality, the stabilization vector also called *hour-glass* part

$$\begin{aligned} \boldsymbol{N}_\gamma &= \frac{1}{8}\,[\,\boldsymbol{I} - (\boldsymbol{N}_{,\xi}\,\boldsymbol{J}_e^{-1}\,)_{|\,0}\,\boldsymbol{X}_{kn}\,](\,\eta\,\zeta\,\boldsymbol{a}_5 + \xi\,\zeta\,\boldsymbol{a}_6 + \xi\,\eta\,\boldsymbol{a}_7 + \xi\,\eta\,\zeta\,\boldsymbol{a}_8\,) \\ &= \eta\,\zeta\,\boldsymbol{\gamma}_1 + \xi\,\zeta\,\boldsymbol{\gamma}_2 + \xi\,\eta\,\boldsymbol{\gamma}_3 + \xi\,\eta\,\zeta\,\boldsymbol{\gamma}_4 \end{aligned} \tag{10.59}$$

is derived after some algebraic manipulations, see Belytschko et al. (1984). The 12 stabilization vectors $\bar{\boldsymbol{\gamma}}$ can now be computed from the components of vectors $\boldsymbol{\gamma}_k$ $(k = 1, 4)$ by using four $\boldsymbol{\gamma}$ vectors for each component. Hence the 8

components of the $\boldsymbol{\gamma}$ vectors yield 12 $\bar{\boldsymbol{\gamma}}$ vectors with $3 \times 8 = 24$ components. Explicitly, the vectors are given by

$$\begin{aligned}
\bar{\boldsymbol{\gamma}}_1 &= \{\gamma_1^1, 0, 0, \gamma_1^2, 0, 0, \dots, \gamma_1^8, 0, 0\}^T \\
\bar{\boldsymbol{\gamma}}_2 &= \{\gamma_2^1, 0, 0, \gamma_2^2, 0, 0, \dots, \gamma_2^8, 0, 0\}^T \\
\bar{\boldsymbol{\gamma}}_3 &= \{\gamma_3^1, 0, 0, \gamma_3^2, 0, 0, \dots, \gamma_3^8, 0, 0\}^T \\
\bar{\boldsymbol{\gamma}}_4 &= \{\gamma_4^1, 0, 0, \gamma_4^2, 0, 0, \dots, \gamma_4^8, 0, 0\}^T \\
\bar{\boldsymbol{\gamma}}_5 &= \{0, \gamma_1^1, 0, 0, \gamma_1^2, 0, \dots, 0, \gamma_1^8, 0\}^T \\
\bar{\boldsymbol{\gamma}}_6 &= \{0, \gamma_2^1, 0, 0, \gamma_2^2, 0, \dots, 0, \gamma_2^8, 0\}^T \\
\bar{\boldsymbol{\gamma}}_7 &= \{0, \gamma_3^1, 0, 0, \gamma_3^2, 0, \dots, 0, \gamma_3^8, 0\}^T \\
\bar{\boldsymbol{\gamma}}_8 &= \{0, \gamma_4^1, 0, 0, \gamma_4^2, 0, \dots, 0, \gamma_4^8, 0\}^T \\
\bar{\boldsymbol{\gamma}}_9 &= \{0, 0, \gamma_1^1, 0, 0, \gamma_1^2, \dots, 0, 0, \gamma_1^8\}^T \\
\bar{\boldsymbol{\gamma}}_{10} &= \{0, 0, \gamma_2^1, 0, 0, \gamma_2^2, \dots, 0, 0, \gamma_2^8\}^T \\
\bar{\boldsymbol{\gamma}}_{11} &= \{0, 0, \gamma_3^1, 0, 0, \gamma_3^2, \dots, 0, 0, \gamma_3^8\}^T \\
\bar{\boldsymbol{\gamma}}_{12} &= \{0, 0, \gamma_4^1, 0, 0, \gamma_4^2, \dots, 0, 0, \gamma_4^8\}^T .
\end{aligned}$$

Here the terms γ_k^m ($k = 1, 4$ and $m = 1, 8$) are the components of the $\boldsymbol{\gamma}$ vectors defined in (10.59).

10.4.2 Weak Form and Linearization

The weak form for the *hour-glass* stabilized 8-node elements follows from the results derived in Sect. 4.2.1. The matrices and vectors are now evaluated using 1 point GAUSS integration. In detail, the internal virtual work is obtained from (4.54)

$$\int_B \delta\mathbf{E} \cdot \mathbf{S}\, dV = \bigcup_{e=1}^{n_e} \sum_{I=1}^{8} \boldsymbol{\eta}_I^T \int_{\Omega_\square} (\, \boldsymbol{B}_{L\,I}^T\, \boldsymbol{S}_e\,)_{|\,0}\ \det \boldsymbol{J}_{|\,0}\, d\square\,, \tag{10.60}$$

where index 0 denotes the evaluation of the integrals at the element midpoint $\boldsymbol{\xi} = \mathbf{0}$. The residual term due to the stabilization vectors is given by

$$G_{stab} = \bigcup_{e=1}^{n_e} \sum_{i=1}^{12} \boldsymbol{\eta}_e^T\, \alpha_i\, (\, \bar{\boldsymbol{\gamma}}_i^T\ \boldsymbol{u}_e\,)\, \bar{\boldsymbol{\gamma}}_i\,. \tag{10.61}$$

The vectors $\boldsymbol{\eta}_e$ and $\boldsymbol{u}_e$ contain all 24 components of the test functions and displacements within element Ω_e,; hence the sum over all element nodes used in (10.60) disappears. By combining both terms and by evaluating (10.60), using the one-point integration, the residual vector of one finite element is given, see also (4.55),

$$\begin{aligned}
\boldsymbol{R}_e\,(\boldsymbol{u}_e) &= \boldsymbol{R}_{e0}\,(\boldsymbol{u}_e) + \boldsymbol{K}_{stab}\, \boldsymbol{u}_e \\
&= 8 \sum_{I=1}^{8} \Big[\, \boldsymbol{B}_{L\,I}^T\, \boldsymbol{S} \Big]_{|\,0}\ \det \boldsymbol{J}_{|\,0} + \sum_{i=1}^{12} \alpha_i\, (\, \bar{\boldsymbol{\gamma}}_i^T\ \boldsymbol{u}_e\,)\, \bar{\boldsymbol{\gamma}}_i\,.
\end{aligned} \tag{10.62}$$

The linearization of the residual vector yields the tangential stiffness matrix which is needed within the NEWTON method. From (4.76),

$$\begin{aligned}\bar{\boldsymbol{K}}_{T_e} &= \bar{\boldsymbol{K}}_{T_{e0}} + \boldsymbol{K}_{stab} \\ &= \sum_{I=1}^{8}\sum_{K=1}^{8} 8 \left[(\nabla_X N_I)^T \, \bar{\boldsymbol{S}} (\nabla_X N_K) + \bar{\boldsymbol{B}}_{L\,I}^T \, \bar{\boldsymbol{D}} \, \bar{\boldsymbol{B}}_{L\,K} \right]_{|\,0} \det \boldsymbol{J}_{|\,0} \\ &\quad + \sum_{i=1}^{12} \alpha_i \, \bar{\boldsymbol{\gamma}}_i \, \bar{\boldsymbol{\gamma}}_i^T \end{aligned} \tag{10.63}$$

is obtained for a one-point integration.

The solution of a problem using the discretized weak form (10.62) depends on the choice of the parameters α_i. The values of α_i do not play a significant role for standard three-dimensional engineering problems in solid mechanics. The parameters can be selected within a certain range and then do not influence the result of the computation. However, when bending dominates the solution behaviour, the solution can depend on the stabilization parameters a_i.

Within the linear theory, it was possible for Kosloff and Frazier (1978) to show that a special choice of the parameter α_i leads to a finite element which is equivalent to the incompatible mode element of Taylor et al. (1976). In that way, a very efficient element with excellent bending behaviour was obtained. For nonlinear problems, there exists no simple way to compute the stabilization parameters. Here the bending solution depends on the parameter α_i, as already shown in Reese (1994) using the example of a simple cantilever under point load. Thus it is desirable to develop a procedure for bending dominated problems in which the parameters α_i can be derived such that a solution dependence disappears. A related method is formulated in Sect. 10.5.3.[1]

10.5 Enhanced Strain Element

It is important to construct finite elements for problems of solid mechanics which can be applied to a wide range of problems. Such elements should be able to model finite strain states for arbitrary elastic and inelastic materials. Furthermore, they should work in the presence of constraints such as incompressibility which lead for standard displacement elements to locking, see Sect. 10.2. Good element performance for bending dominated structural problems is also necessary when arbitrary structural parts have to be discretized and simulated using three-dimensional solids. Last but not least

[1] The stabilized finite element formulation derived above for the initial configuration can also be developed with respect to the current configuration. In that case, all quantities have to be mapped to the current configuration using the standard transformations, see Sect. 4.2.3.

elements should be robust when large mesh distortion occur due to large deformations.

In the last twenty years, many different finite elements were developed for finite deformation problems and successfully applied to special problem classes. One example is the Q1-P0 element which is well suited for incompressible materials.

In case of linear elastic applications, there exist many possibilities for the design of finite elements which are locking free, have good bending performance and are robust against mesh distortions, see e.g. the hybrid formulations Pian and Sumihara (1984), or the incompatible mode elements of Taylor et al. (1976). Also the stabilized elements from Kosloff and Frazier (1978) have the same good properties.[2] A variational formulation of the discretization using the incompatible modes was derived in Simo and Rifai (1990). This concept has the advantage that it can also be applied to nonlinear problems like finite elastic or inelastic deformations.

The concept followed in the work by Simo and Armero (1992) and Simo et al. (1993b) is based on the principle of Hu–Washizu. The finite elements derived by this formulation are called *enhanced strain* or *enhanced assumed strain* (EAS) elements.

While very well suited for linear elastic problem, the enhanced strain elements do not provide a solution for all problem classes mentioned above in nonlinear applications. The elements become instable under compression which was shown for the first time in Wriggers and Reese (1994), see also Wriggers and Reese (1996). Stabilized versions of the enhanced strain elements have been formulated to overcome this disadvantage. However, until lately, these stabilizations could not solve all defects found in Wriggers and Reese (1996) in a satisfactory way. Refined ansatz functions for the enhanced modes solved the instabilities for two-dimensional problems in the compression range, see Korelc and Wriggers (1996a) and Glaser and Armero (1997). But they lead to instabilities in tension states. An in-depth discussion of these phenomena and possible solutions can be found in Sect. 10.5.4.

In the following section, elements based on the enhanced strain concept will be derived, using on one hand the shape functions provided in Simo and Armero (1992) and on the other hand shape functions stemming from a Taylor series expansion which was developed in Wriggers and Hueck (1996).

10.5.1 General Concept and Formulation

The development of the nonlinear version of the *enhanced strain* elements is generally based on a mixed variational principle. Following Simo and Armero (1992), Hu–Washizu's principle is applied, see Sect. 3.4.3. Here

[2] An interesting observation is that the aforementioned formulations can be transferred to each other, see Bischoff et al. (1999a). Thus different mechanical formulations lead to the same element stiffness matrices.

HU–WASHIZU principle is formulated in terms of the deformation $\boldsymbol{\varphi}$, the deformation gradient $\mathbf{F}$ and the first PIOLA–KIRCHHOFF stress tensor $\mathbf{P}$ which act as independent variables

$$\begin{aligned} \Pi(\boldsymbol{\varphi}, \mathbf{F}, \mathbf{P}) &= \int_B [\, W(\mathbf{F}) + \mathbf{P} \cdot (\operatorname{Grad} \boldsymbol{\varphi} - \mathbf{F}) \,] \, dV \\ &\quad - \int_B \boldsymbol{\varphi} \cdot \rho_0 \, \hat{\mathbf{b}} \, dV - \int_{\partial B_\sigma} \boldsymbol{\varphi} \cdot \hat{\mathbf{t}} \, dA \,. \end{aligned} \tag{10.64}$$

$W(\mathbf{F})$ denotes the strain energy function of the elastic material under consideration. This formulation is equivalent to the principle provided in (3.300). To simplify notation, the last two terms in (10.64) which describe external forces will be combined and denoted by P_{EXT}.[3]

The variational principle of HU–WASHIZU was formulated in this way in order to be able to additively decompose the deformation gradient, see Simo and Armero (1992). In this decomposition, the local deformation gradient $\operatorname{Grad} \boldsymbol{\varphi}$ is complemented by the independent gradient $\bar{\mathbf{F}}$

$$\mathbf{F} = \operatorname{Grad} \boldsymbol{\varphi} + \bar{\mathbf{F}} \,. \tag{10.65}$$

Thus the deformation gradient $\mathbf{F}$ is enriched by the *enhanced* gradient $\bar{\mathbf{F}}$ which can be incompatible with the deformation. With Eq. (10.65), relation

$$\Pi(\boldsymbol{\varphi}, \bar{\mathbf{F}}, \mathbf{P}) = \int_B [\, W(\mathbf{F}) - \mathbf{P} \cdot \bar{\mathbf{F}} \,] \, dV - P_{EXT} \tag{10.66}$$

is obtained from (10.64). Its variation yields

$$\begin{aligned} \int_B \operatorname{Grad} \boldsymbol{\eta} \cdot \frac{\partial W}{\partial \mathbf{F}} \, dV - \delta P_{EXT} &= 0, \\ \int_B \delta \bar{\mathbf{F}} \cdot \left(-\mathbf{P} + \frac{\partial W}{\partial \mathbf{F}} \right) dV &= 0, \\ \int_B \delta \mathbf{P} \cdot \bar{\mathbf{F}} \, dV &= 0 \,. \end{aligned} \tag{10.67}$$

$\operatorname{Grad} \boldsymbol{\eta}$ denotes the variation of the deformation gradient, see (3.289). The first equation denotes the weak form of equilibrium. The second equations

[3] It is also possible to formulate the HU–WASHIZU principle in other work conjugate variables. Examples are the 2nd PIOLA–KIRCHHOFF stress tensor and the GREEN–LAGRANGIAN strain tensor $\mathbf{E}$ or the application of the BIOT stress tensor $\mathbf{T}_B$ together with the right stretch tensor $\mathbf{U}$. From the viewpoint of continuum mechanics, these formulations are equivalent. However, due to the fact that the strain measures $\mathbf{F}$, $\mathbf{E}$ and $\mathbf{U}$ are different, their enhancement will lead to different finite element approximations and discretizations.

leads to the constitutive relation. Equation $(10.67)_3$ represents an orthogonality condition between the stress tensor and the variation of the enhanced gradient $\bar{\mathbf{F}}$.

Equations (10.65) and (10.67) provide a variational basis which can be employed to incorporate the incompatible (enhanced) modes in a consistent way to the finite element formulation.

An efficient implementation of the enhanced element can be obtained by transforming all quantities in (10.67) to the current configuration, see also Sect. 4.2.3. By computing the deformation gradient from (10.65), relation

$$\begin{aligned} \int_B \nabla^S \boldsymbol{\eta} \cdot \left(2\,\mathbf{F}\,\frac{\partial W}{\partial \mathbf{C}}\,\mathbf{F}^T \right) dV - \delta P_{EXT} &= 0, \\ \int_B \delta\,\bar{\mathbf{h}}^S \cdot \left(-\boldsymbol{\tau} + 2\,\mathbf{F}\,\frac{\partial W}{\partial \mathbf{C}}\,\mathbf{F}^T \right) dV &= 0, \\ \int_B \delta\,\boldsymbol{\tau} \cdot \bar{\mathbf{h}}\, dV &= 0 \end{aligned} \tag{10.68}$$

is deduced based on (10.67). Here the gradient $\nabla^S \boldsymbol{\eta} = \mathrm{sym}\,[\mathrm{Grad}\,\boldsymbol{\eta}\,\mathbf{F}^{-1}]$ is the symmetric part of the variation of the deformation gradient with respect to the current configuration. The tensor $\mathbf{C} = \mathbf{F}^T\mathbf{F}$ is the right Cauchy–Green strain tensor, see (3.15). The enhanced gradient in the current configuration is computed from $\bar{\mathbf{h}} = \bar{\mathbf{F}}\mathbf{F}^{-1}$. The symmetric Kirchhoff stress tensor follows with the 1st Piola–Kirchhoff stresses from $\boldsymbol{\tau} = \mathbf{P}\,\mathbf{F}^T$ or with (3.84) from the 2nd Piola–Kirchhoff stress tensor: $\boldsymbol{\tau} = \mathbf{F}\,\mathbf{S}\,\mathbf{F}^T$. Since $\boldsymbol{\tau}$ is a symmetric tensor, only the symmetric parts of the deformation gradient $\nabla^S \boldsymbol{\eta}$ and the enhanced gradient $\bar{\mathbf{h}}^S$ contribute to the scalar product with the Kirchhoff stresses in Eq. (10.68).

To complete the model, a strain energy function W is needed. Different variants can be found for hyperelastic materials in Sect. 3.3.1. The Kirchhoff stresses follow then from the 2nd Piola–Kirchhoff stresses via (3.104).

10.5.2 Discretization of the Enhanced Strain Element

An isoparametric ansatz, see (4.4), is introduced to discretize the displacement field and the geometry of the current configuration in (10.65)

$$\mathbf{x}_e = \mathbf{X}_e + \mathbf{u}_e = \sum_{I=1}^{n} N_I(\boldsymbol{\xi})\,\boldsymbol{x}_I \qquad \text{with} \quad x_I = X_I + u_I\,. \tag{10.69}$$

In the two-dimensional case, the bilinear shape functions (4.28) are applied. In case of three-dimensional discretizations, the shape functions (4.40) are used.

The conforming part of the deformation gradient can now be determined from (10.69). With (4.8) and (4.11), the deformation gradient follows

$$\operatorname{Grad} \boldsymbol{\varphi}_e = \sum_{I=1}^{n} \boldsymbol{x}_I \otimes \nabla_X N_I(\boldsymbol{\xi}) = \sum_{I=1}^{n} \boldsymbol{x}_I \otimes \boldsymbol{J}_e^{-T} \nabla_\xi N_I(\boldsymbol{\xi}) \,. \tag{10.70}$$

For the enhanced part of the deformation gradient, an interpolation has to be selected which even can be incompatible. Following Glaser and Armero (1997), a product form is defined for the enriched part $\bar{\mathbf{F}}$

$$\bar{\mathbf{F}} = \mathbf{F}_0 \, \bar{\mathbf{M}} \, \boldsymbol{\alpha} \,. \tag{10.71}$$

$\boldsymbol{\alpha}$ denote the *enhanced* parameters, $\bar{\mathbf{M}}$ contains the interpolation functions. $\mathbf{F}_0$ is the constant part of the conform deformation gradient (10.70), which is evaluated at the element midpoint

$$\mathbf{F}_0 = \sum_{I=1}^{n} \boldsymbol{x}_I \otimes \nabla_X N_I(\mathbf{0}) \,. \tag{10.72}$$

The ansatz (10.71) fulfils the requirements for objectivity of the enhanced element formulation for arbitrary interpolations $\bar{\mathbf{M}}$, see Glaser and Armero (1997).[4]

The interpolations of the enriched part $\bar{\mathbf{M}}$ are related to the initial configuration of a finite element Ω_e. Since the incompatible interpolations have to be formulated with respect to the reference configuration $\Omega_\square$, like the isoparametric interpolations, $\bar{\mathbf{M}}$ has to be transformed to $\Omega_\square$ (for the relevant notation, see Fig. 4.3). This is performed by using the tensor transformation

$$\bar{\mathbf{M}} = \frac{j_0}{j} \, \boldsymbol{J}_0 \, \boldsymbol{M}(\boldsymbol{\xi}) \, \boldsymbol{J}_0^{-1} \,. \tag{10.73}$$

Here J_0 defines the mapping between Ω_e and $\Omega_\square$, see (4.7), which is evaluated at the element midpoint ($\boldsymbol{\xi} = \mathbf{0}$). The determinant of the transformation is denoted by $j = \det \boldsymbol{J}_e$. Its evaluation at the element midpoint is denoted by $j_0 = \det \boldsymbol{J}_0$.

Now the interpolation for the enhanced modes have to be selected. These can be incompatible since no derivatives of the enriched deformation gradient appear in (10.67). In general, the ansatz

$$\boldsymbol{M}(\boldsymbol{\xi})\boldsymbol{\alpha} = \sum_{L=1}^{n_{enh}} \boldsymbol{M}_L(\boldsymbol{\xi}) \, \alpha_L \tag{10.74}$$

[4] This representation deviates from the form advocated in Simo and Armero (1992) in such a way that $\bar{\mathbf{M}}$ was introduced as a gradient and hence could be interpolated without using $\mathbf{F}_0$, see also Exercise 10.1.

can be introduced with n_{enh} interpolations for the additional incompatible modes. The ansatz can be written for two-dimensional elements in the compact form

$$\boldsymbol{M}(\boldsymbol{\xi})\,\boldsymbol{\alpha} = \begin{bmatrix} M_1(\xi,\eta)\;\alpha_1 & M_2(\xi,\eta)\;\alpha_2 \\ M_3(\xi,\eta)\;\alpha_3 & M_4(\xi,\eta)\;\alpha_4\,. \end{bmatrix}. \tag{10.75}$$

The interpolations M_L have to obey the orthogonality condition $(10.67)_3$ within the element

$$\int_{\Omega_e} \delta\mathbf{P}_e \cdot \bar{\mathbf{F}}_e \, d\Omega = 0\,. \tag{10.76}$$

By assuming constant stresses in Ω_e, condition

$$\int_{\Omega_e} \bar{\mathbf{M}} \, d\Omega = 0 \tag{10.77}$$

is obtained based on (10.71). It yields with (10.73)

$$\int_{\Omega_\square} \boldsymbol{M}(\boldsymbol{\xi}) \, d\square = 0\,. \tag{10.78}$$

The interpolations M_L in (10.75) have to fulfil this condition which is the case for polynomials with uneven exponents. Hence the simplest interpolation with four enhanced or incompatible modes is given by

$$\boldsymbol{M}(\boldsymbol{\xi})^{2D}\,\boldsymbol{\alpha} = \sum_{L=1}^{4} \boldsymbol{M}(\boldsymbol{\xi})_L^{2D}\,\alpha_L = \begin{bmatrix} \xi\,\alpha_1 & \eta\,\alpha_2 \\ \xi\,\alpha_3 & \eta\,\alpha_4 \end{bmatrix}. \tag{10.79}$$

The finite element based on this ansatz is called Q1/E4 element, see Simo and Armero (1992). This element is equivalent in the linear case with the incompatible mode element by Taylor et al. (1976).

The corresponding interpolation for the three-dimensional case leads to an ansatz for the enhanced deformation gradient with nine modes

$$\boldsymbol{M}^{3D}\,\boldsymbol{\alpha} = \sum_{L=1}^{9} \boldsymbol{M}(\boldsymbol{\xi})_L^{3D}\,\alpha_L = \begin{bmatrix} \xi\,\alpha_1 & \eta\,\alpha_2 & \zeta\,\alpha_3 \\ \xi\,\alpha_4 & \eta\,\alpha_5 & \zeta\,\alpha_6 \\ \xi\,\alpha_7 & \eta\,\alpha_8 & \zeta\,\alpha_9 \end{bmatrix}. \tag{10.80}$$

It is simply the extension of the two-dimensional interpolation and yields the so-called Q1/E9 element. As already shown in Simo et al. (1993b), this ansatz is not sufficient to prevent locking. Thus additional enhanced modes have to be introduced in order to prevent volume locking. The related element has 12 incompatible modes and hence is called Q1/E12 element.

The matrix formulation of the enhanced finite element is based on a description of the deformation gradient in vector form. It will be developed here

for the two-dimensional case. A different formulation is provided in Exercise 10.1 in detail.

Basis of the implementation is the mixed form (10.67) with respect to the initial configuration, but form (10.68) could also be employed which is referred to the current configuration. Essential for an efficient implementation is the use of formulations which lead to sparse matrices. As already discussed in the standard formulation of isoparametric elements, see Sects. 4.2.2 and 4.2.4, the formulation (10.68) with respect to the current configurations provides the most efficient variant.

The quantities $\nabla^S \boldsymbol{\eta}$ and $\delta \mathbf{h}^S$ have to be discretized in (10.68). Furthermore, the KIRCHHOFF stresses are computed from $\boldsymbol{\tau} = 2\,\mathbf{F}\,\frac{\partial W}{\partial C}\,\mathbf{F}^T$ using (10.65). The variation of the deformation dependent part of the deformation gradient follows with (3.32) within the element Ω_e in the current configuration as

$$\nabla \boldsymbol{\eta}_e = \operatorname{Grad} \boldsymbol{\eta}_e \, \mathbf{F}_e^{-1} = \left[\sum_{I=1}^{n} \boldsymbol{\eta}_I \otimes \nabla_X N_I(\boldsymbol{\xi}) \right] \mathbf{F}_e^{-1} \,. \tag{10.81}$$

Here the enriched deformation gradient has to be introduced for $\mathbf{F}$, see (10.65). The symmetrical part follows as in (4.94). Its matrix form is given by

$$\nabla^S \boldsymbol{\eta}_e = \sum_{I=1}^{n} \begin{bmatrix} N_{I,1} & 0 \\ 0 & N_{I,2} \\ N_{I,2} & N_{I,1} \end{bmatrix} \left\{ \begin{matrix} \eta_1 \\ \eta_2 \end{matrix} \right\}_I = \sum_{I=1}^{n} \boldsymbol{B}_I \, \boldsymbol{\eta}_I \,, \tag{10.82}$$

where the derivatives have to be determined using (10.81). For the enhanced modes, the vector form is given by

$$\delta \bar{\mathbf{h}}_e^S = \sum_{L=1}^{n_{enh}} \begin{bmatrix} M_{11}^L \\ M_{22}^L \\ M_{12}^L + M_{21}^L \end{bmatrix} \delta\alpha_L = \sum_{I=L}^{n_{enh}} \boldsymbol{G}_L \, \delta\alpha_L \,. \tag{10.83}$$

In this relation, the components $M_{11}^L \,, M_{12}^L \,, M_{21}^L$ and M_{22}^L have to be computed based on (10.73) and (10.74) from

$$\bar{\boldsymbol{M}}_L = \begin{bmatrix} M_{11}^L & M_{12}^L \\ M_{21}^L & M_{22}^L \end{bmatrix} = \mathbf{F}_0 \, \frac{j_0}{j} \, \mathbf{J}_0 \, \boldsymbol{M}(\boldsymbol{\xi})_L \, \mathbf{J}_0^{-1} \, \mathbf{F}_e^{-1} \,. \tag{10.84}$$

$\boldsymbol{M}(\boldsymbol{\xi})_L$ denotes the L^{th} mode, see (10.79). The weak form (10.68) can now be rewritten as

$$\begin{aligned} \bigcup_{e=1}^{n_e} \left[\sum_I \delta \boldsymbol{\eta}_I{}^T \int_{\Omega_e} \boldsymbol{B}_I{}^T \, \boldsymbol{\tau}_e \, d\Omega \right] - \delta P_{EXT} \;&=\; 0 \\ \sum_L \delta\alpha_L \int_{\Omega_e} \boldsymbol{G}_L{}^T \, \boldsymbol{\tau}_e \, d\Omega \;&=\; 0 \,. \end{aligned} \tag{10.85}$$

Note that $(10.68)_3$ is directly fulfilled by construction of the enhanced interpolations, see (10.73).

The solution of this nonlinear algebraic equation system will be obtained by NEWTON'S method. Hence the linearization of (10.85) has to be derived. Analogous to the procedure given in Sect. 4.2.4, the incremental equation system

$$\begin{bmatrix} \boldsymbol{K}_{u\,u} & \boldsymbol{K}_{u\,\alpha} \\ \boldsymbol{K}_{\alpha\,u} & \boldsymbol{K}_{\alpha\,\alpha} \end{bmatrix} \left\{ \begin{array}{c} \Delta \boldsymbol{u} \\ \Delta \boldsymbol{\alpha} \end{array} \right\} = - \left\{ \begin{array}{c} \boldsymbol{G}_u \\ \boldsymbol{G}_\alpha \end{array} \right\} \tag{10.86}$$

can be deduced. In this form, the sub matrices are given by

$$\begin{aligned}
\mathbf{K}_{u\,u} &= \bigcup_{e=1}^{n_e} \sum_{I=1}^{n} \sum_{K=1}^{n} \int_{\Omega_e} [\boldsymbol{B}_I^T \, \boldsymbol{D}^{MR} \, \boldsymbol{B}_K + (\overline{\nabla}_x N_I)^T \, \boldsymbol{\tau}_e \, \overline{\nabla}_x N_K] \, d\Omega, \\
\mathbf{K}_{u\,\alpha} &= \bigcup_{e=1}^{n_e} \sum_{I=1}^{n} \sum_{M=1}^{n_{enh}} \int_{\Omega_e} [\, {\boldsymbol{B}_I}^T \, \boldsymbol{D}^{MR} \, \boldsymbol{G}_M \\
&\quad + (\overline{\nabla}_x N_I)^T \, \boldsymbol{\tau}_e \, \boldsymbol{G}_M + (\overline{\nabla}_x N_I\big|_0)^T \, \boldsymbol{\tau}_e \, \boldsymbol{G}_M] \, d\Omega, \\
\mathbf{K}_{\alpha\,\alpha} &= \bigcup_{e=1}^{n_e} \sum_{L=1}^{n_{enh}} \sum_{M=1}^{n_{enh}} \int_{\Omega_e} [\, \boldsymbol{G}_L^T \, \boldsymbol{D}^{MR} \, \boldsymbol{G}_M + \bar{\boldsymbol{M}}_L \boldsymbol{\tau} \cdot \bar{\boldsymbol{M}}_M \,] \, d\Omega.
\end{aligned} \tag{10.87}$$

The residuals $\boldsymbol{G}_u$ and $\boldsymbol{G}_\alpha$ follow directly from (10.85). As in the previous equations, the derivatives have to be determined with respect to x via (10.81). The definition of $\boldsymbol{D}^{MR}$ can be found in (4.113). $(\overline{\nabla}_x N_I\big|_0)$ denotes the evaluation of the gradient at the element midpoint, see also (10.72). For the solution of equation system (10.86), block elimination can be employed. It provides an efficient implementation since $\boldsymbol{K}_{\alpha\alpha}$ can be inverted directly on element level due to the incompatible interpolation functions. This procedure is explicitly shown in Exercise 10.1.

Exercise 10.1: Derive the discretization and resulting matrix formulation for a two-dimensional 4-node element based on the HU–WASHIZU principle. Use for the derivatives of the shape functions and for the interpolation of the enhanced modes a TAYLOR series expansion up to order 2 with respect to the element mid point. The element has to be constructed for finite elastic deformations.

Solution: Within the element Ω_e, the displacements will be approximated by isoparametric shape functions. The use of a TAYLOR series expansion of order 2 for the standard shape functions and enhanced mode interpolations leads to explicit expressions for the gradients. Within the range of small strains, it was shown in Hueck and Wriggers (1995) that this method can be applied to all terms which are associated with the enhanced element.

In case of finite deformations explicit expressions are developed for the standard and the enhanced displacement gradients in (10.65). These gradients

are related to the initial configuration $\mathbf{X}$. After that the equations will be transformed to the current configuration $\mathbf{x}$.

The bilinear isoparametric form functions (4.28) are used for the interpolation

$$N_I(\xi,\eta) = \frac{1}{4}\,(1+\xi\,\xi_I)(1+\eta\,\eta_I) = \frac{1}{4}\,(\,1\,+\,\xi_I\,\xi+\,\eta_I\,\eta\,+\,\xi_I\eta_I\,\xi\eta\,)\,. \quad (10.88)$$

ξ_I and η_I are the coordinates of node I in the ξ–η reference configuration of the element. The coordinates within the element are given by

$$\begin{aligned} X &= a_0 + a_1\,\xi + a_2\,\xi\eta + a_3\,\eta \\ Y &= b_0 + b_1\,\xi + b_2\,\xi\eta + b_3\,\eta, \end{aligned} \quad (10.89)$$

where the constants a_i are defined as follows

$$\begin{aligned} a_0 &= \frac{1}{4}\sum_{I=1}^{4} X_I\,, & a_1 &= \frac{1}{4}\sum_{I=1}^{4} \xi_I\,X_I\,, \\ a_2 &= \frac{1}{4}\sum_{I=1}^{4} \xi_I\,\eta_I\,X_I\,, & a_3 &= \frac{1}{4}\sum_{I=1}^{4} \eta_I\,X_I\,. \end{aligned}$$

The constants b_i are computed in an analogous way where X_I is exchanged by Y_I. The deformation gradient within the element follows with (10.88)

$$\operatorname{Grad}\boldsymbol{\varphi}_e = \sum_{I=1}^{4} \begin{bmatrix} N_{I,X}\,x_I & N_{I,Y}\,x_I \\ N_{I,X}\,y_I & N_{I,Y}\,y_I \end{bmatrix}. \quad (10.90)$$

In this relation, x_I and y_I are the coordinates of node I in the current configuration. In Eq. (10.90), the derivatives of the form functions have to be computed with respect to X and Y. A Taylor series expansion up to order 1 yields with respect to the element midpoint $\xi = \eta = 0$

$$N_I = N_I|_0 + \left.\frac{\partial N_I}{\partial X}\right|_0 (\,X - X_0\,) + \left.\frac{\partial N_I}{\partial Y}\right|_0 (\,Y - Y_0\,) + N_{\gamma I}. \quad (10.91)$$

The remaining higher order terms are denoted by $N_{\gamma I}$. From (10.88) $N_I|_0 = 1/4$ is obtained. The evaluation of the chain rule at the element midpoint leads to

$$\begin{Bmatrix} \left.\dfrac{\partial N_I}{\partial X}\right|_0 \\ \left.\dfrac{\partial N_I}{\partial Y}\right|_0 \end{Bmatrix} = \boldsymbol{J}_0^{-1} \begin{Bmatrix} \left.\dfrac{\partial N_I}{\partial \xi}\right|_0 \\ \left.\dfrac{\partial N_I}{\partial \eta}\right|_0 \end{Bmatrix}. \quad (10.92)$$

$\mathbf{J}_0$ is the Jacobi matrix $\boldsymbol{J}$ evaluated at the element midpoint. The derivatives of the shape functions can be computed at the element mid point by, as shown in Hueck and Wriggers (1995),

$$\left.\frac{\partial N_I}{\partial X}\right|_0 = \frac{1}{4\,j_0}\,(\quad b_3\,\xi_I - b_1\,\eta_I\,)\,, \tag{10.93}$$

$$\left.\frac{\partial N_I}{\partial Y}\right|_0 = \frac{1}{4\,j_0}\,(\,-a_3\,\xi_I + a_1\,\eta_I\,)\,. \tag{10.94}$$

The determinant $\boldsymbol{J}$ is given by $j = j_0 + j_1\,\xi + j_2\,\eta$ with

$$j_0 = a_1\,b_3 - a_3\,b_1\,, \qquad j_1 = a_1\,b_2 - a_2\,b_1 \qquad \text{and} \quad j_2 = a_2\,b_3 - a_3\,b_2\,.$$

This leads to $\det \boldsymbol{J}_0 = j_0$. The solution of (10.91) yields with (10.93) and (10.94) after some algebraic manipulations the higher order term

$$N_{\gamma I} = \gamma_I\,\xi\eta \qquad \text{with} \quad \gamma_I = \frac{1}{4}\left(\,\xi_I\eta_I - \frac{j_2}{j_0}\,\xi_I - \frac{j_1}{j_0}\,\eta_I\,\right), \tag{10.95}$$

where the so-called stabilization- or γ-vector has been introduced, see also Sect. 10.4 and Belytschko et al. (1984).

The interpolation functions for the enhanced gradient $\bar{\mathbf{F}}$ in (10.65) are determined analogous to (10.90). Wilson et al. (1973) have introduced the classical incompatible modes by

$$M_1 = (\,1 - \xi^2\,), \qquad M_2 = (\,1 - \eta^2\,)\,. \tag{10.96}$$

These represent a discontinuous interpolation between different elements Ω_e. An expansion using the TAYLOR series around the element midpoint yields, for the incompatible modes,

$$M_L = \left.M_L\right|_0 + \left.\frac{\partial M_L}{\partial X}\right|_0 (\,X - X_0\,) + \left.\frac{\partial M_L}{\partial Y}\right|_0 (\,Y - Y_0\,) + M_{\gamma L}\,. \tag{10.97}$$

The constant term is $\left.M_I\right|_0 = 1$. By the chain rule, it can be shown that all terms of first order are zero in (10.97). The remaining terms of higher order in (10.97) are

$$M_{\gamma 1} = -\xi^2 \qquad \text{and} \quad M_{\gamma 2} = -\eta^2\,. \tag{10.98}$$

Now the higher order terms in Eqs. (10.95) and (10.96) will be expanded in X and Y by a TAYLOR series of second order with respect to the element midpoint. To simplify notation, the terms are combined in $\mathbf{q}^T = \{\,q_1,\,q_2,\,q_3\} = \{\,\xi^2,\,\xi\eta,\,\eta^2\,\}$. TAYLOR series expansion yields

$$\mathbf{q} = \frac{1}{2}\left(\left.\frac{\partial^2\mathbf{q}}{\partial X^2}\right|_0 \Delta X^2 + 2\left.\frac{\partial^2\mathbf{q}}{\partial X\partial Y}\right|_0 \Delta X\,\Delta Y + \left.\frac{\partial^2\mathbf{q}}{\partial Y^2}\right|_0 \Delta Y^2\right) + \mathbf{r}_3 \tag{10.99}$$

with $\Delta X = X - X_0$ and $\Delta Y = Y - Y_0$. Constant terms and terms of first order do not appear in this equation since $\mathbf{q}$ only consists of terms of higher order, which appear as remainders in the expansion of N_I (10.91) and M_L (10.97). The term $\mathbf{r}_3$ contains terms of third order and will be neglected in the

following derivations. The computation of the second derivatives in (10.99) are described in detail in Hueck and Wriggers (1995). They lead to the form

$$
\begin{aligned}
N_{\gamma I} &= -\frac{1}{j_0^2}\,[\,b_1\,b_3\,\Delta X^2 - (\,a_1\,b_3 + a_3\,b_1\,)\,\Delta X\,\Delta Y + a_1\,a_3\,\Delta Y^2\,]\,\gamma_I\,, \\
M_{\gamma 1} &= -\frac{1}{j_0^2}\,[\,b_3^2\,\Delta X^2 - 2\,a_3\,b_3\,\Delta X\,\Delta Y + a_3^2\,\Delta Y^2\,]\,, \\
M_{\gamma 2} &= -\frac{1}{j_0^2}\,[\,b_1^2\,\Delta X^2 - 2\,a_1\,b_1\,\Delta X\,\Delta Y + a_1^2\,\Delta Y^2\,]\,.
\end{aligned}
\tag{10.100}
$$

The shape functions and the incompatible interpolations can be approximated by these equations and by (10.93) and (10.94). Finally, with Eqs. (10.91) and (10.100), the derivatives of the shape functions with respect to X and Y yield

$$
\begin{aligned}
N_{I,X} &= N_{I,X}|_0 + N_{I\gamma,X} \\
&= \frac{1}{4\,j_0}\,(\,b_3\,\xi_I - b_1\,\eta_I\,) - \frac{1}{j_0^2}\,[\,2\,b_1\,b_3\,\Delta X - (a_1\,b_3 + a_3\,b_1)\Delta Y\,]\,\gamma_I\,.
\end{aligned}
\tag{10.101}
$$

Since Eq. (10.89) leads to $\Delta X = a_1\xi + a_2\xi\eta + a_3\eta$ and $\Delta Y = b_1\xi + b_2\xi\eta + b_3\eta$, explicit expressions can be derived for the derivatives of N_I with respect to X

$$
N_{I,X} = \frac{1}{4\,j_0}\,(\,b_3\,\xi_I - b_1\,\eta_I\,) + \frac{1}{j_0}\,\left[\,-b_1\xi + \frac{1}{j_0}\,(j_1\,b_3 - j_2\,b_1)\,\xi\eta + b_3\,\eta\right]\,\gamma_I\,.
\tag{10.102}
$$

Analogously the derivatives of N_I with respect to Y follow as

$$
N_{I,Y} = \frac{1}{4\,j_0}\,(\,a_1\,\eta_I - a_3\,\xi_I\,) + \frac{1}{j_0}\,\left[\,a_1\xi + \frac{1}{j_0}\,(j_2\,a_1 - j_1\,a_3)\,\xi\eta - a_3\,\eta\right]\,\gamma_I\,.
\tag{10.103}
$$

The derivatives of the incompatible modes are obtained using (10.97) and (10.100)

$$
\begin{aligned}
M_{1,X} &= -\frac{2}{j_0}\,b_3\,\left(\,\xi + \frac{j_2}{j_0}\,\xi\,\eta\right)\,, \qquad M_{1,Y} = \frac{2}{j_0}\,a_3\,\left(\,\xi + \frac{j_2}{j_0}\,\xi\,\eta\right)\,, \\
M_{2,X} &= \frac{2}{j_0}\,b_1\,\left(\,\eta + \frac{j_1}{j_0}\,\xi\,\eta\right)\,, \qquad M_{2,Y} = -\frac{2}{j_0}\,a_1\,\left(\,\eta + \frac{j_1}{j_0}\,\xi\,\eta\right)\,.
\end{aligned}
\tag{10.104}
$$

It is possible to compute the gradients (10.90) and (10.105) with respect to the reference configuration $\mathbf{X}$ by using expressions (10.102) to (10.104). For the enhanced deformation, gradient $\bar{\mathbf{F}}$ follows

$$
\bar{\mathbf{F}}_e = \sum_{L=1}^{2} \boldsymbol{\alpha}_L\,\bar{\boldsymbol{G}}_L^T \quad \text{with} \quad \boldsymbol{\alpha}_L = \left\{\begin{array}{c} \alpha_L \\ \phi_L \end{array}\right\} \quad \text{and} \quad \bar{\boldsymbol{G}}_L = \left\{\begin{array}{c} M_{L,X} \\ M_{L,Y} \end{array}\right\}\,,
\tag{10.105}
$$

where α_L and ϕ_L are the variables with respect to the coordinate directions related to the enhanced modes.

Remark 10.2: In Eqs. (10.102), (10.103) and (10.104) only the constant term J_0 of the JACOBI determinant appears in the denominator. This expression is proportional to the element area and cannot become zero or negative, even when an element is highly distorted. Hence this formulation is more robust against geometric mesh distortion.

By using (10.68) as a basis for the nonlinear finite element formulation, the gradients have to be transformed to the current configuration. The standard displacement gradient is transformed by $\nabla \mathbf{u} = (\mathrm{Grad}\, \mathbf{u})\, \mathbf{F}^{-1}$ to the spatial displacement gradient

$$\nabla \mathbf{u}_e = \sum_{I=1}^{4} \begin{bmatrix} N_{I,x}\, u_I & N_{I,y}\, u_I \\ N_{I,x}\, v_I & N_{I,y}\, v_I \end{bmatrix} \tag{10.106}$$

with the nodal displacements u_I and v_I. The derivatives of the shape functions with respect to $\mathbf{x}$ follow for the two-dimensional case in explicit form

$$\begin{Bmatrix} N_{I,x} \\ N_{I,y} \end{Bmatrix} = \frac{1}{\det \mathbf{F}_e} \begin{Bmatrix} F_{22}\, N_{I,X} - F_{21}\, N_{I,Y} \\ -F_{12}\, N_{I,X} + F_{11}\, N_{I,Y} \end{Bmatrix} . \tag{10.107}$$

Here F_{ik} are the components of the deformation gradient $\mathbf{F}$, see (10.65).

At the same time the enhanced gradient is transformed to the current configuration. This yields – as for the displacement gradient – $\bar{\mathbf{h}} = \bar{\mathbf{F}}\, \mathbf{F}^{-1}$. Together with (10.105), it follows

$$\bar{\mathbf{h}}_e = \sum_{L=1}^{2} \boldsymbol{\alpha}_L\, \bar{\boldsymbol{g}}_L^T \quad \text{with} \quad \bar{\boldsymbol{g}}_L = \mathbf{F}_e^{-T}\, \bar{\boldsymbol{G}}_L \,, \tag{10.108}$$

where

$$\bar{\boldsymbol{g}}_L = \begin{Bmatrix} M_{L,x} \\ M_{L,y} \end{Bmatrix} = \frac{1}{\det \mathbf{F}} \begin{Bmatrix} F_{22}\, M_{L,X} - F_{21}\, M_{L,Y} \\ -F_{12}\, M_{L,X} + F_{11}\, M_{L,Y} \end{Bmatrix} \tag{10.109}$$

is valid. Thus the enhanced gradient is transformed to the current configuration in a similar way as the displacement gradient.

The discretization of the weak form (10.68) requires, for plane strain, the matrices

$$\boldsymbol{\tau} = \begin{Bmatrix} \tau_{11} \\ \tau_{22} \\ \tau_{12} \end{Bmatrix} , \mathbf{b} = \begin{Bmatrix} b_{11} \\ b_{22} \\ b_{12} \end{Bmatrix} , \nabla^S \boldsymbol{\eta} = \begin{Bmatrix} \eta_{,x} \\ \eta_{,y} \\ \eta_{,y} + \eta_{,x} \end{Bmatrix} , \delta\bar{\mathbf{h}}^S = \begin{Bmatrix} \delta h_{11} \\ \delta h_{22} \\ \delta h_{12} + \delta h_{21} \end{Bmatrix} . \tag{10.110}$$

From the constitutive relation (3.120), the KIRCHHOFF stresses

$$\boldsymbol{\tau}_e = \begin{Bmatrix} \tau_{11} \\ \tau_{22} \\ \tau_{12} \end{Bmatrix}_e = \frac{\Lambda}{2} [\, J^2 - 1\,] \begin{Bmatrix} 1 \\ 1 \\ 0 \end{Bmatrix} + \mu \left[\begin{Bmatrix} b_{11} \\ b_{22} \\ b_{12} \end{Bmatrix} - \begin{Bmatrix} 1 \\ 1 \\ 0 \end{Bmatrix} \right] \tag{10.111}$$

can be deduced. In this expression, the discrete approximation for the left CAUCHY–GREEN tensor $\mathbf{b}$ is given by

$$\mathbf{b}_e = \left\{ \begin{array}{c} (F_{11})^2 + (F_{12})^2 \\ (F_{22})^2 + (F_{21})^2 \\ F_{11}\,F_{21} + F_{12}\,F_{22} \end{array} \right\} . \tag{10.112}$$

The components of the deformation gradient $\mathbf{F}$ are computed from (10.65) together with (10.90) and (10.105)

$$\left[\begin{array}{cc} F_{11} & F_{12} \\ F_{21} & F_{22} \end{array} \right]_e = \sum_{I=1}^{4} \left[\begin{array}{cc} N_{I,X}\,x_I & N_{I,Y}\,x_I \\ N_{I,X}\,y_I & N_{I,Y}\,y_I \end{array} \right] + \sum_{L=1}^{2} \left[\begin{array}{cc} M_{L,X}\,\alpha_L & M_{L,Y}\,\alpha_L \\ M_{L,X}\,\phi_L & M_{L,Y}\,\phi_L \end{array} \right] \tag{10.113}$$

within an element Ω_e. The variation of the symmetric displacement gradient is provided in Ω_e by

$$\nabla^S \boldsymbol{\eta}_e = \sum_{I=1}^{4} \boldsymbol{B}_I\,\boldsymbol{\eta}_I = \sum_{I=1}^{4} \left[\begin{array}{cc} N_{I,x} & 0 \\ 0 & N_{I,y} \\ N_{I,y} & N_{I,x} \end{array} \right] \left\{ \begin{array}{c} \eta_{x\,I} \\ \eta_{y\,I} \end{array} \right\} . \tag{10.114}$$

This defines the $\mathbf{B}$-matrix, see also (4.94). The derivatives of the shape functions are computed from (10.107) with (10.102) and (10.103) with respect to the current configuration. Analogously, the variation of the enhanced displacement gradient $\bar{\mathbf{h}}$ is given with (10.108) and (10.105) by

$$\delta\bar{\mathbf{h}}_e^S = \sum_{L=1}^{2} \boldsymbol{G}_L\,\delta\boldsymbol{\alpha}_L = \sum_{L=1}^{2} \left[\begin{array}{cc} M_{L,x} & 0 \\ 0 & M_{L,y} \\ M_{L,y} & M_{L,x} \end{array} \right] \left\{ \begin{array}{c} \delta\alpha_L \\ \delta\phi_L \end{array} \right\} . \tag{10.115}$$

The relations (10.104) and (10.109) have to be applied in (10.115) to compute $M_{L,x}$ and $M_{L,y}$.

The discretization of (10.68) yields with (10.110) to (10.115) the residuals of the enhanced element

$$\left. \begin{array}{l} \bigcup\limits_{e=1}^{n_e} \left\{ \sum\limits_{I=1}^{4} \boldsymbol{\eta}_I^T \int\limits_{\Omega_e} \boldsymbol{B}_I^T\,\boldsymbol{\tau}_e\,d\Omega \right\} - \delta P_{EXT} = 0 \\ \qquad\qquad \sum\limits_{L=1}^{2} \delta\boldsymbol{\alpha}_L^T \int\limits_{\Omega_e} \boldsymbol{G}_L^T\,\boldsymbol{\tau}_e\,d\Omega = 0 \end{array} \right\} \Rightarrow \begin{array}{ll} \boldsymbol{g}_u(\,\boldsymbol{u},\,\boldsymbol{\alpha}\,) & = \mathbf{0} \\ \boldsymbol{g}_\alpha^e(\,\boldsymbol{u},\,\boldsymbol{\alpha}\,) & = \mathbf{0}\,, \end{array} \tag{10.116}$$

where the abbreviations $\mathbf{g}_u = \mathbf{0}$ and $\mathbf{g}_\alpha^e = \mathbf{0}$ were introduced for the first and second equation. The last equation in (10.68) has only to be fulfilled on element level. This follows from the fact that the interpolation functions for the enhanced modes are discontinuous over the element domains. Furthermore, the interpolation of the stress field can be selected in (10.67) and (10.68) such that $(10.68)_3$ is automatically fulfilled, see Simo and Armero (1992).

Remark 10.3: Equation $(10.116)_2$ leads for constant stresses to the condition $\int_{\Omega_e} \bar{\mathbf{G}}_L \, dV = 0$. This has to be considered in order to fulfil the patch test for piecewise constant stress fields. With the enhanced functions in (10.104), this condition is fulfilled exactly when the following approximation is used for the integration

$$\int_B f(x,y)\, dV = \int_{-1}^{1}\int_{-1}^{1} f(\xi,\eta)\, j \, d\xi \, d\eta \approx \int_{-1}^{1}\int_{-1}^{1} f(\xi,\eta)\, j_0 \, d\xi \, d\eta.$$

Due to this the use of j_0 instead of j is important for the mapping onto the reference configuration within this element formulation, see also (10.78).

Newton's method is usually applied to solve the nonlinear algebraic equation system (10.116) for the unknown displacements $\boldsymbol{u}$ and the enhanced variables $\boldsymbol{\alpha}$, see Sect. 5.1.1. This iterative scheme requires the linearization of (10.116). As was shown in Sect. 3.5.3, Eq. (10.68) is transformed for this operation to the initial configuration

$$\begin{aligned} G_u &= \int_B \operatorname{Grad}\boldsymbol{\eta} \cdot \left(2\,\mathbf{F}\,\frac{\partial W}{\partial \mathbf{C}} \right) dV - \delta P_{EXT} = 0\,, \\ G_\alpha &= \int_B \delta\,\bar{\mathbf{F}} \cdot \left(2\,\mathbf{F}\,\frac{\partial W}{\partial \mathbf{C}} \right) dV = 0\,. \end{aligned} \tag{10.117}$$

The linearization will be denoted by $\Delta(\bullet)$, as introduced in Sect. 3.5.3.

The linearization of $\mathbf{F}$ yields with (10.65) $\Delta\mathbf{F} = \operatorname{Grad}\Delta\mathbf{u} + \Delta\bar{\mathbf{F}}$. This relation is used to linearize $\mathbf{C} = \mathbf{F}^T\mathbf{F}$

$$\Delta\mathbf{C} = \Delta(\mathbf{F}^T\mathbf{F}) = [\,(\operatorname{Grad}\Delta\mathbf{u}\,)^T + \Delta\bar{\mathbf{F}}^T\,]\,\mathbf{F} + \mathbf{F}^T\,[\,\operatorname{Grad}\Delta\mathbf{u} + \Delta\bar{\mathbf{F}}\,]\,. \tag{10.118}$$

Use of the linearized kinematical quantities in (10.117) leads to

$$\begin{aligned} \Delta G_u &= \int_B \operatorname{Grad}\boldsymbol{\eta} \cdot 2 \left[(\operatorname{Grad}\Delta\mathbf{u} + \Delta\bar{\mathbf{F}}\,)\,\frac{\partial W}{\partial \mathbf{C}} + \mathbf{F}\,\frac{\partial^2 W}{\partial \mathbf{C}\,\partial \mathbf{C}}\Delta\mathbf{C} \right] dV = 0, \\ \Delta G_\alpha &= \int_B \delta\,\bar{\mathbf{F}} \cdot 2 \left[(\operatorname{Grad}\Delta\mathbf{u} + \Delta\bar{\mathbf{F}}\,)\,\frac{\partial W}{\partial \mathbf{C}} + \mathbf{F}\,\frac{\partial^2 W}{\partial \mathbf{C}\,\partial \mathbf{C}}\Delta\mathbf{C} \right] dV = 0\,. \end{aligned} \tag{10.119}$$

This result is pushed forward to the current configuration. Employing the relation between the 2nd Piola–Kirchhoff stress tensor $\mathbf{S}$ and the Kirchhoff stress tensor $\boldsymbol{\tau} = \mathbf{F}\,\mathbf{S}\,\mathbf{F}^T$, see (3.84), and using the incremental material tensor in the current configuration $\mathfrak{c}$, see (3.245), relations

$$
\begin{aligned}
\Delta g_u &= \int_B \left\{ \nabla^S \boldsymbol{\eta} \cdot \mathfrak{c}\,[\,\nabla^S(\Delta\mathbf{u})\,] + \nabla^S \boldsymbol{\eta}\, \nabla^S(\Delta\mathbf{u}) \cdot \boldsymbol{\tau} \right\} dV \\
&\quad + \int_B \left\{ \nabla^S \boldsymbol{\eta} \cdot \mathfrak{c}\,[\,\Delta\bar{\mathbf{h}}\,] + \nabla^S \boldsymbol{\eta}\, \Delta\bar{\mathbf{h}} \cdot \boldsymbol{\tau} \right\} dV = 0, \\
\Delta g_\alpha &= \int_B \left\{ \delta\bar{\mathbf{h}}^S \cdot \mathfrak{c}\,[\,\nabla^S(\Delta\mathbf{u})\,] + \bar{\mathbf{h}}^S\, \nabla^S(\Delta\mathbf{u}) \cdot \boldsymbol{\tau} \right\} dV \\
&\quad + \int_B \left\{ \delta\bar{\mathbf{h}}^S \cdot \mathfrak{c}\,[\,\Delta\bar{\mathbf{h}}\,] + \delta\bar{\mathbf{h}}\, \Delta\bar{\mathbf{h}} \cdot \boldsymbol{\tau} \right\} dV = 0
\end{aligned}
\tag{10.120}
$$

are deduced after some algebraic manipulations.

In case of a plane strain state, the explicit expression for the constitutive tensor (3.120), see also (3.271), is given by

$$
\boldsymbol{D} = \begin{bmatrix} e_1 & e_2 & 0 \\ e_2 & e_1 & 0 \\ 0 & 0 & g \end{bmatrix} \quad \text{with} \quad \begin{aligned} e_1 &= \mu + \Lambda \\ e_2 &= \Lambda\, J^2 \\ g &= \mu - \tfrac{\Lambda}{2}\,[\,J^2 - 1\,]\,. \end{aligned} \tag{10.121}
$$

The operators for determining $\nabla^S \boldsymbol{\eta}$ and $\delta\bar{\mathbf{h}}^S$ are stated in discrete form in (10.114) and (10.115). The same operators can also be applied for the determination of $\nabla^S(\Delta\mathbf{u})$ and $\Delta\bar{\mathbf{h}}^S$. With this notation, the following tangent matrices are defined as

$$
\begin{aligned}
\boldsymbol{K}_{u\,u} &= \bigcup_{e=1}^{n_e} \sum_{I=1}^{4} \sum_{J=1}^{4} \int_{\Omega_e} \left[\boldsymbol{B}_I^T\, \boldsymbol{D}\, \boldsymbol{B}_J + G_{IJ}^1\, \mathbf{I}_{2\times 2} \right] d\Omega \\
\boldsymbol{K}_{u\,\alpha} &= \bigcup_{e=1}^{n_e} \sum_{I=1}^{4} \sum_{L=1}^{2} \int_{\Omega_e} \left[\boldsymbol{B}_I^T\, \boldsymbol{D}\, \boldsymbol{G}_L + G_{IL}^2\, \mathbf{I}_{2\times 2} \right] d\Omega \qquad (10.122) \\
\boldsymbol{K}_{\alpha\,\alpha} &= \bigcup_{e=1}^{n_e} \sum_{L=1}^{2} \sum_{M=1}^{2} \int_{\Omega_e} \left[\boldsymbol{G}_L^T\, \boldsymbol{D}\, \boldsymbol{G}_M + G_{LM}^3\, \mathbf{I}_{2\times 2} \right] d\Omega \qquad (10.123)
\end{aligned}
$$

with

$$
\begin{aligned}
G_{IJ}^1 &= <\, N_{I,x}\,,\, N_{I,y}\, > \begin{bmatrix} \tau_{11} & \tau_{12} \\ \tau_{21} & \tau_{22} \end{bmatrix} \begin{Bmatrix} N_{J,x} \\ N_{J,y} \end{Bmatrix} \\
G_{IL}^2 &= <\, N_{I,x}\,,\, N_{I,y}\, > \begin{bmatrix} \tau_{11} & \tau_{12} \\ \tau_{21} & \tau_{22} \end{bmatrix} \begin{Bmatrix} M_{L,x} \\ M_{L,y} \end{Bmatrix} \\
G_{LM}^3 &= <\, M_{L,x}\,,\, M_{L,y}\, > \begin{bmatrix} \tau_{11} & \tau_{12} \\ \tau_{21} & \tau_{22} \end{bmatrix} \begin{Bmatrix} M_{M,x} \\ M_{M,y} \end{Bmatrix}.
\end{aligned}
$$

Since the interpolation functions for the enhanced strains are discontinuous, it is possible to invert the matrix $\boldsymbol{K}_{\alpha\,\alpha}$ on element level. By writing the equation system for one element as

$$\begin{aligned} \boldsymbol{K}^e_{u\,u}\,\Delta\boldsymbol{u}^e + \boldsymbol{K}^e_{u\,\alpha}\,\Delta\boldsymbol{\alpha}^e &= -\boldsymbol{g}^e_u \\ \boldsymbol{K}^e_{\alpha\,u}\,\Delta\boldsymbol{u}^e + \boldsymbol{K}^e_{\alpha\,\alpha}\,\Delta\boldsymbol{\alpha}^e &= -\boldsymbol{g}^e_\alpha \end{aligned} \tag{10.124}$$

a block elimination technique, as employed in Simo and Rifai (1990), is efficient in combination with NEWTON'S method to solve (10.124). Within this procedure, the variables $\boldsymbol{\alpha}^e$ are eliminated on element level

$$\Delta\boldsymbol{\alpha}^e = -\boldsymbol{K}^{e\,-1}_{\alpha\,\alpha}\,(\,\boldsymbol{K}^e_{\alpha\,u}\Delta\boldsymbol{u}^e + \boldsymbol{g}^e_\alpha\,)\,. \tag{10.125}$$

This leads to the displacement formulation

$$(\,\boldsymbol{K}^e_{u\,u} - \boldsymbol{K}^e_{u\,\alpha}\,\boldsymbol{K}^{e\,-1}_{\alpha\,\alpha}\,\boldsymbol{K}^e_{\alpha\,u}\,)\Delta\boldsymbol{u}^e = -\boldsymbol{g}^e_u + \boldsymbol{K}^e_{u\,\alpha}\,\boldsymbol{K}^{e\,-1}_{\alpha\,\alpha}\,\boldsymbol{g}^e_\alpha \tag{10.126}$$

and hence to the definition of the element residual and tangent matrix for the enhanced element

$$\hat{\boldsymbol{g}}_u = \boldsymbol{g}^e_u - \boldsymbol{K}^e_{u\,\alpha}\,\boldsymbol{K}^{e\,-1}_{\alpha\,\alpha}\,\boldsymbol{g}^e_\alpha \quad \text{and} \quad \hat{\boldsymbol{K}}_{u\,u} = \boldsymbol{K}^e_{u\,u} - \boldsymbol{K}^e_{u\,\alpha}\,\boldsymbol{K}^{e\,-1}_{\alpha\,\alpha}\,\boldsymbol{K}^e_{\alpha\,u}\,. \tag{10.127}$$

An efficient implementation which avoids the storage of $\boldsymbol{K}^{e\,-1}_{\alpha\,\alpha}\,\boldsymbol{K}^e_{\alpha\,u}$ and $\boldsymbol{K}^{e\,-1}_{\alpha\,\alpha}\,\boldsymbol{g}_\alpha$ on element level can be found in Simo et al. (1993b).

10.5.3 Combination of Enhanced Formulation and Hour-Glass Stabilization

A possibility in which the advantage of the stabilized *hour-glass* elements of Belytschko et al. (1984) (high efficiency) is combined with the advantage of the *enhanced strain* elements (*locking* free behaviour) was developed in Reese et al. (1998) and has been refined since then in Reese (2003) and Reese (2005). Staring point of this development are the relations (10.62) and (10.63). These lead after assembly to the nonlinear equation

$$\boldsymbol{R}_0 + \boldsymbol{K}_{stab}\,\boldsymbol{v} = \boldsymbol{P} \tag{10.128}$$

and its linearization

$$(\,\boldsymbol{K}_{T0} + \boldsymbol{K}_{stab}\,)\,\Delta\boldsymbol{v} = \boldsymbol{P} - \boldsymbol{R}_0 - \boldsymbol{K}_{stab}\,\boldsymbol{v}\,. \tag{10.129}$$

In order to derive the explicit form of $\boldsymbol{K}_{stab}$ for this formulation, the deformation gradient $\boldsymbol{F}$ and its enhanced part $\bar{\boldsymbol{F}}$ in (10.65) is written as

$$\begin{aligned} \boldsymbol{F}_e &= \boldsymbol{B}\,\boldsymbol{x}_e \qquad \text{Grad}\,\boldsymbol{\eta}_e = \boldsymbol{B}\,\boldsymbol{\eta}_e \quad \text{and} \\ \bar{\boldsymbol{F}}_e &= \boldsymbol{G}\,\boldsymbol{\alpha}_e \qquad \delta\bar{\boldsymbol{F}}_e = \boldsymbol{G}\,\delta\boldsymbol{\alpha}_e\,, \end{aligned} \tag{10.130}$$

where vector notation is introduced.

In the two-dimensional case, the explicit form

$$\mathrm{Grad}\,\boldsymbol{\eta}_e = \left\{ \begin{array}{c} \eta_{1,1} \\ \eta_{1,2} \\ \eta_{2,1} \\ \eta_{2,2} \end{array} \right\} = \sum_{I=1}^{4} \boldsymbol{B}_I\, \boldsymbol{\eta}_I = \sum_{I=1}^{4} \left[\begin{array}{cc} N_{I,X} & 0 \\ N_{I,Y} & 0 \\ 0 & N_{I,X} \\ 0 & N_{I,Y} \end{array} \right] \left\{ \begin{array}{c} \eta_{X\,I} \\ \eta_{Y\,I} \end{array} \right\} \quad (10.131)$$

is obtained for the variation of $\boldsymbol{F}_e$ using the ansatz (10.88). This relation can be written in a compact way as

$$\mathrm{Grad}\,\boldsymbol{\eta}_e = [\,\boldsymbol{B}_1\,,\boldsymbol{B}_2\,,\boldsymbol{B}_3\,,\boldsymbol{B}_4\,] \left\{ \begin{array}{c} \eta_{X\,1} \\ \eta_{Y\,1} \\ \ldots \\ \eta_{X\,4} \\ \eta_{Y\,4} \end{array} \right\} = \boldsymbol{B}\,\boldsymbol{\eta}_e\,. \quad (10.132)$$

Starting from the TAYLOR series expansion of the shape functions, see (10.91), the $\boldsymbol{B}$-matrix can be split into linear and *hour-glass* parts. This leads after Reese and Wriggers (2000) to

$$\boldsymbol{B} = \boldsymbol{j}(\,\boldsymbol{B}_{lin}\,\boldsymbol{M}_{lin} + \boldsymbol{B}_{hg}\,\boldsymbol{M}_{hg}\,)\,. \quad (10.133)$$

For two-dimensions, the matrices in (10.133) have the form

$$\boldsymbol{j} = \left[\begin{array}{cccc} \frac{\partial \xi}{\partial X} & \frac{\partial \eta}{\partial X} & 0 & 0 \\ 0 & 0 & \frac{\partial \xi}{\partial Y} & \frac{\partial \eta}{\partial Y} \\ \frac{\partial \xi}{\partial Y} & \frac{\partial \eta}{\partial Y} & 0 & 0 \\ 0 & 0 & \frac{\partial \xi}{\partial X} & \frac{\partial \eta}{\partial X} \end{array} \right], \quad (10.134)$$

$$\boldsymbol{B}_{lin} = \left[\begin{array}{cccccc} 0 & 1 & 0 & 0 & 0 & 0 \\ 0 & 0 & 1 & 0 & 0 & 0 \\ 0 & 0 & 0 & 0 & 1 & 0 \\ 0 & 0 & 0 & 0 & 0 & 1 \end{array} \right], \qquad \boldsymbol{B}_{hg} = \left[\begin{array}{cc} \eta & 0 \\ \xi & 0 \\ 0 & \eta \\ 0 & \xi \end{array} \right], \quad (10.135)$$

and

$$\begin{aligned} \boldsymbol{M}_{lin}^T &= \left[\begin{array}{cccccc} \boldsymbol{N}_0 & \boldsymbol{N}_{,X\,0} & \boldsymbol{N}_{,Y\,0} & \boldsymbol{O} & \boldsymbol{O} & \boldsymbol{O} \\ \boldsymbol{O} & \boldsymbol{O} & \boldsymbol{O} & \boldsymbol{N}_0 & \boldsymbol{N}_{,X\,0} & \boldsymbol{N}_{,Y\,0} \end{array} \right], \\ \boldsymbol{M}_{hg}^T &= \left[\begin{array}{cc} \boldsymbol{\gamma} & \boldsymbol{O} \\ \boldsymbol{O} & \boldsymbol{\gamma} \end{array} \right]. \end{aligned} \quad (10.136)$$

The components $N_I|_0$, $\frac{\partial N_I}{\partial X}\big|_0$ and $\frac{\partial N_I}{\partial Y}\big|_0$, computed in (10.91), (10.93) and (10.94), are contained in vectors $\boldsymbol{N}_0$, $\boldsymbol{N}_{,X\,0}$ and $\boldsymbol{N}_{,Y\,0}$. In vector $\boldsymbol{\gamma}$, the components of the γ vector, see (10.95), are assembled.

The enhanced strain parts will now be specified based on the application of the ansatz (10.96). The variation of the enhanced strain gradient in (10.65) follows analogously to (10.131)

$$\delta\bar{\mathbf{F}}_e = \left\{ \begin{array}{c} \delta\bar{F}_{11} \\ \delta\bar{F}_{12} \\ \delta\bar{F}_{21} \\ \delta\bar{F}_{22} \end{array} \right\} = \sum_{L=1}^{2} \boldsymbol{G}_L \, \delta\boldsymbol{\varphi}_L = \sum_{I=1}^{4} \left[\begin{array}{cc} M_{L,X} & 0 \\ M_{L,Y} & 0 \\ 0 & M_{L,X} \\ 0 & M_{L,Y} \end{array} \right] \left\{ \begin{array}{c} \delta\varphi_L \\ \delta\phi_L \end{array} \right\} . \tag{10.137}$$

This can be written in compact form

$$\delta\bar{\mathbf{F}}_e = [\, \boldsymbol{G}_1 \, , \boldsymbol{G}_2 \,] \left\{ \begin{array}{c} \delta\varphi_1 \\ \delta\phi_1 \\ \delta\varphi_2 \\ d\phi_2 \end{array} \right\} = \boldsymbol{G} \, \delta\boldsymbol{\alpha}_e \, . \tag{10.138}$$

Since the approximation for the enhanced strain term does not contain constant and linear parts, the $\boldsymbol{G}$ matrix can be expressed by a TAYLOR series expansion

$$\boldsymbol{G} = \boldsymbol{j} \, \hat{\boldsymbol{G}} \quad \text{with} \quad \hat{\boldsymbol{G}} = \left[\begin{array}{cccc} \xi & 0 & 0 & 0 \\ 0 & \eta & 0 & 0 \\ 0 & 0 & \xi & 0 \\ 0 & 0 & 0 & \eta \end{array} \right] . \tag{10.139}$$

The variational equation (10.67) follows from the HU–WASHIZU principle. Its discretization uses the above defined matrices

$$\begin{aligned} \bigcup_{e=1}^{n_e} \boldsymbol{\eta}_e^T \int_{\Omega_e} [\boldsymbol{j} (\boldsymbol{B}_{lin} \, \boldsymbol{M}_{lin} + \boldsymbol{B}_{hg} \, \boldsymbol{M}_{hg})]^T \, \boldsymbol{P}_e \, d\Omega - \delta P_{EXT} &= 0 \\ \delta\boldsymbol{\alpha}_e^T \int_{\Omega_e} (\boldsymbol{j} \, \hat{\boldsymbol{G}})^T \, \boldsymbol{P}_e \, d\Omega &= 0. \end{aligned} \tag{10.140}$$

For the fulfillment of the last equation in (10.67), the ansatz $\boldsymbol{G} = \frac{j_0}{j} \, \boldsymbol{j}_0 \, \hat{\boldsymbol{G}}$ has to be selected for distorted element geometry. This leads with the incremental constitutive matrix $\boldsymbol{A} = \frac{\partial^2 W}{\partial F \, \partial F}$, for the linearization of the second equation of (10.140), to

$$\begin{aligned} \delta\boldsymbol{\alpha}_e^T \Bigg[\int_{\Omega_e} \hat{\boldsymbol{G}}^T \hat{\boldsymbol{A}} \boldsymbol{B}_{lin} \, d\Omega \, \boldsymbol{M}_{lin} \, \Delta \, \boldsymbol{u}_e + \int_{\Omega_e} \hat{\boldsymbol{G}}^T \hat{\boldsymbol{A}} \boldsymbol{B}_{hg} \, d\Omega \, \boldsymbol{M}_{hg} \, \Delta \, \boldsymbol{u}_e \\ + \int_{\Omega_e} \hat{\boldsymbol{G}}^T \hat{\boldsymbol{A}} \hat{\boldsymbol{G}} \, d\Omega \, \Delta \, \boldsymbol{\alpha}_e \Bigg] = -\delta\boldsymbol{\alpha}_e^T \int_{\Omega_e} \hat{\boldsymbol{G}}^T \, \hat{\boldsymbol{P}}_e \, d\Omega \, . \end{aligned} \tag{10.141}$$

Here the abbreviation $\hat{\boldsymbol{A}} = \boldsymbol{j}^T \, \boldsymbol{A} \, \boldsymbol{j}$ was introduced together with the abbreviation for the 1st PIOLA–KIRCHHOFF stress tensor $\hat{\boldsymbol{P}}_e = \boldsymbol{j}^T \, \boldsymbol{P}_e$. The form (10.141) can now be simplified by assuming that $\hat{\boldsymbol{A}}$, $\hat{\boldsymbol{P}}$ and $\boldsymbol{j} \, dV$ are constant within an element Ω_e. These assumptions are approximations for arbitrary element geometries. The assumption of constant stress states and rhomboidal

element forms enables an exact evaluation of (10.141). Hence the solution converges for arbitrary meshes when a sufficient number of finite elements is used. In that case, the stress fields in the elements are nearly constant. Due to this simplification, the first integral in (10.141) disappears, since $\boldsymbol{B}_{lin}$ is constant and $\hat{\boldsymbol{G}}$ is linear in ξ and η. With the definitions

$$\boldsymbol{K}_{\alpha\, u} = \int_{\Omega_e} \hat{\boldsymbol{G}}^T \hat{\boldsymbol{A}}_0 \boldsymbol{B}_{hg}\, d\Omega_0 \quad \text{and} \quad \boldsymbol{K}_{\alpha\, \alpha} = \int_{\Omega_e} \hat{\boldsymbol{G}}^T \hat{\boldsymbol{A}} \hat{\boldsymbol{G}}\, d\Omega_0, \tag{10.142}$$

the matrix relation

$$\Delta\, \boldsymbol{\alpha} = -\boldsymbol{K}_{\alpha\, \alpha}^{-1} \boldsymbol{K}_{\alpha\, u}\, \boldsymbol{M}_{hg}\, \Delta \boldsymbol{v} \tag{10.143}$$

follows for the incremental enhanced variables $\Delta\boldsymbol{\alpha}$ on element level. In (10.142), the index $()_0$ denotes evaluation of a quantity at element midpoint (this is equivalent to a 1-point-integration). The increments of the gradients follow from (10.133) and (10.139) with (10.143)

$$\Delta \boldsymbol{F} + \Delta\, \bar{\boldsymbol{F}} = \boldsymbol{j}\, (\, \boldsymbol{B}_{lin}\, \boldsymbol{M}_{lin} + \boldsymbol{B}_{stab}\, \boldsymbol{M}_{hg}\,)\, \Delta \boldsymbol{v}\,, \tag{10.144}$$

where the new $\boldsymbol{B}$-matrix, $\boldsymbol{B}_{stab}$, is defined by

$$\boldsymbol{B}_{stab} = \boldsymbol{B}_{hg} - \hat{\boldsymbol{G}}\, \boldsymbol{K}_{\alpha\, \alpha}^{-1} \boldsymbol{K}_{\alpha\, u}\,. \tag{10.145}$$

This relation can be inserted in the linearized form of $(10.140)_1$. It leads to the tangent matrix, by noting that $\int_{\Omega_e} \boldsymbol{B}_{lin}^T \hat{\boldsymbol{A}}_0 \boldsymbol{B}_{stab}\, d\Omega_0$ and $\int_{\Omega_e} \hat{\boldsymbol{G}}^T \hat{\boldsymbol{A}}_0 \boldsymbol{B}_{stab}\, d\Omega_0$ are zero,

$$\boldsymbol{K}_T = \boldsymbol{M}_{lin}^T\, \boldsymbol{K}_0\, \boldsymbol{M}_{lin} + \boldsymbol{M}_{hg}^T\, \boldsymbol{K}_{stab}\, \boldsymbol{M}_{hg} \tag{10.146}$$

with

$$\boldsymbol{K}_0 = \int_{\Omega_e} \boldsymbol{B}_{lin}^T \hat{\boldsymbol{A}}_0 \boldsymbol{B}_{lin}\, d\Omega_0 \quad \text{and} \quad \boldsymbol{K}_{stab} = \int_{\Omega_e} \boldsymbol{B}_{stab}^T \hat{\boldsymbol{A}}_0 \boldsymbol{B}_{stab}\, d\Omega_0\,. \tag{10.147}$$

Since $\boldsymbol{B}_{lin}$ is constant, $\boldsymbol{K}_0$ is integrated exactly by a 1-point-GAUSS integration. $\boldsymbol{K}_{stab}$ can be integrated analytically. Thus an efficient computation of the tangent matrix $\boldsymbol{K}_T$ is possible. A further advantage is that the constitutive tensor has to be evaluated only at the element midpoint. Since the element volume is also computed using the element midpoint, the element is insensitive against mesh distortions.

Since the first matrix in (10.146) is equivalent to matrix $\boldsymbol{K}_{T0}$ (10.129), the second matrix in (10.146) can be interpreted as stabilization matrix which is here computed by using the enhanced formulation. With this all matrices in (10.129) are known.

Since a constant stabilization matrix is used within the concept of stabilization, see Sect. 10.4, the stabilization matrix in (10.146) also has to be kept constant during the NEWTON iterations within a load step. For large

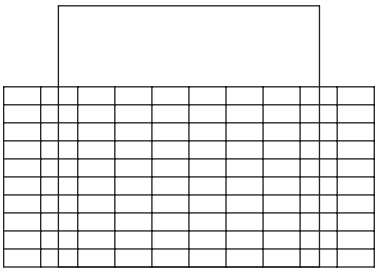

Fig. 10.2a Homogeneous deformation

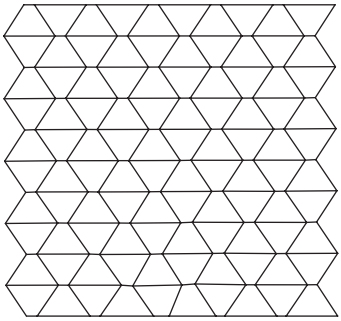

Fig. 10.2b *Hourglass* eigenvector

load steps, however, the stabilization matrix in (10.146) is not optimal in the sense of the enhanced strain method, since e.g. the incremental constitutive tensor may change. Then a post-iteration is required to update the matrix according to the computed deformation and stress state. Such procedure can be viewed as an UZAWA algorithm known from optimization, see e.g. Luenberger (1984). In a recent paper, Reese (2005) presented a new formulation which basically overcomes this problem.

10.5.4 Instabilities Related to Enhanced Elements

Enhanced strain elements were developed over the last 15 years for finite strain problems which include bending dominated response or incompressible behaviour. The advantage of this element formulation is its relatively simple implementation in which complex constitutive equations for finite elastic and inelastic strains can be included. An additional advantage is a good coarse mesh accuracy for different applications. However, there is one disadvantage which is, in the classical formulation of enhanced strain elements, related to instability, see Wriggers and Reese (1994) and Wriggers and Reese (1996). In these papers, it was shown that a block under homogeneous pressure state will lead to a non-physical instability which is related to the enhanced element formulation, see Fig. 10.2a for the problem definition. This instability occurs at a finite deformation state, independently on the constitutive equation.[5]

By applying loading and boundary conditions as depicted in Fig. 10.2a, the loss of uniqueness of the solution occurs and the tangent matrix becomes singular. The eigenmode related to the zero eigenvalue of the tangent stiffness has the form shown in Fig. 10.2b which is well known as hour-glass mode.

[5] Enhanced elements derived for geometrical linear elastic problems are known to be stable for all strain and stress states. However, a even a geometrically linear formulation of the enhanced strain element with an inelastic constitutive equation can depict such instable behaviour.

Thus the instability has nothing to do with the stability problems as discussed in Chap. 7. It can be shown, see below, that the enhanced strain element is rank deficient for this deformation state. This loss of rank can of course also be observed under more complex loading states where pressure occurs locally or for different types of material behaviour.

Interesting enough this phenomena will even occur for a single element. Hence an analytical investigation of this element behaviour is feasable in which all matrices can be presented in closed form.

Here one element will be investigated, assuming hyperelastic constitutive behaviour. A compressible Neo–Hooke material is selected where the strain energy, after (3.116) and (3.118), is given in terms of the principal strains λ_i^2 of the right Cauchy–Green tensor, see (3.15), as

$$W = \frac{1}{2}\mu\,[\,(\lambda_1^2 + \lambda_2^2 + \lambda_3^2) - 3\,] - \mu \ln J + \frac{\Lambda}{4}\,(\,J^2 - 1 - 2\ln J\,)\,. \qquad (10.148)$$

$J = \lambda_1\,\lambda_2\,\lambda_3$ denotes the Jacobi determinant of the deformation gradient.

A homogeneous plain strain state is considered in a rectangular plate, see Fig. 10.2a. Thus it is possible to perform the analysis with respect to the principal strains since the principal directions coincide in this case with the cartesian coordinates. From the strain energy, the 1st Piola–Kirchhoff stresses $\mathbf{P} = \sum_{i=1}^{3} P_i\,\mathbf{n}_i \otimes \mathbf{N}_i$, can be computed, see e.g. Ogden (1984), as

$$P_i = \frac{\partial W}{\partial \lambda_i} = \frac{1}{\lambda_i}\,\left[\,\mu\,(\lambda_i^2 - 1) + \frac{\Lambda}{2}\,(J^2 - 1)\right]\,. \qquad (10.149)$$

Furthermore, the coefficients of the incremental constitutive tensor related to a formulation using $\mathbf{P}$ are needed. After some algebra and analogous to the derivation in (3.265), the incremental constitutive tensor follows with (10.149) from $\mathbb{A}_{iJkL} = \partial P_{iJ} \,/\, \partial F_{kL}$. Hence the non-zero elements of this tensor are given with respect to the principal strains with ($i\,,j = 1\,,2$ and $i \neq j$) as

$$\begin{aligned}
\mathbb{A}_{iiii} &= \mu\,\left(1 + \frac{1}{\lambda_i^2}\right) + \frac{\Lambda}{2\,\lambda_i^2}\,(J^2 + 1) \\
\mathbb{A}_{iijj} &= \Lambda\,J \\
\mathbb{A}_{ijij} &= \mu \\
\mathbb{A}_{ijji} &= \frac{1}{\lambda_i\,\lambda_j}\,\left[\,\mu + \frac{\Lambda}{2}\,(1 - \lambda_i^2\,\lambda_j^2)\right]\,,
\end{aligned} \qquad (10.150)$$

where it is not necessary to distinguish between derivations with respect to the initial- and current configuration.

As already mentioned, it is sufficient to show the rank deficiency for a single finite element. Here an isoparametric bilinear element will be considered which is chosen such that the local $\xi\,,\eta$-axis coincide with the global $X\,,Y$-axis in Fig. 4.2. Hence initial- and reference configuration are the same, see

Fig. 10.3a. For such a discretization all vectors and matrices can be presented explicitly in closed form. The bilinear shape functions are given in this special case in terms of the cartesian coordinates

$$N_I(X\,,Y) = \frac{1}{4}\,(1 + X\,X_I)(1 + Y\,Y_I)\,. \tag{10.151}$$

This leads directly to the derivatives needed for the computation of the deformation gradient after (10.131)

$$N_{I,X} = \frac{X_I}{4}\,(\,1 + Y_I\,Y\,) \quad \text{and} \quad N_{I,Y} = \frac{Y_I}{4}\,(\,1 + X_I\,X\,)\,. \tag{10.152}$$

Hence the $\boldsymbol{B}_I$ matrix in (10.131) is linear in X and Y.

The deformation gradient is enhanced in Eq. (10.65) by $\bar{\mathbf{F}}$. Using the interpolation of the incompatible modes $M_L(X\,,Y)$, see Taylor et al. (1976) and (10.96), it follows for the derivatives in the enhanced gradient (10.137)

$$M_{1,X} = -X\,, \quad M_{1,Y} = 0\,, \quad M_{2,X} = 0 \quad \text{and} \quad M_{2,Y} = -Y\,. \tag{10.153}$$

Now the first two equations of the mixed formulation (10.67) can be formulated with this interpolation. Since a plain stress state is assumed ($P_{33} = 0$), the four stress components

$$\boldsymbol{P}^T = \{\,P_{11}\,,P_{12}\,,P_{21}\,,P_{22}\,\} \tag{10.154}$$

have to be determined. These components of $\boldsymbol{P}$ can be obtained from (10.149) using the deformation gradient from (10.65). This leads to the weak form of the single element Ω_e in Fig. 10.3a

$$\sum_{I=1}^{4} \boldsymbol{\eta}_I^T \int_{\Omega_e} \boldsymbol{B}_I^T\,\boldsymbol{P}\,d\Omega - \delta P_{EXT} \quad = 0$$

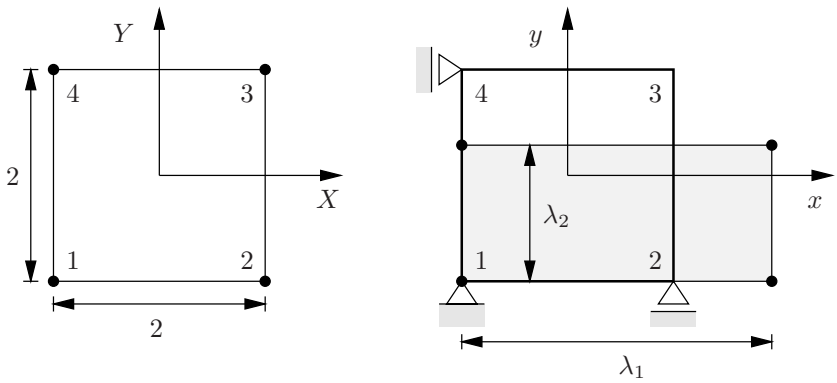

Fig. 10.3 Finite element and homogeneous deformation

$$\sum_{L=1}^{2} \delta\boldsymbol{\varphi}_L^T \int\limits_{\Omega_e} \boldsymbol{G}_L^T \boldsymbol{P}\, d\Omega \quad = 0 \tag{10.155}$$

which is referred to the initial configuration. In case of a homogeneous stress field, the stress P_{22} is constant and $P_{11} = P_{12} = P_{21} = 0$. This yields

$$\begin{aligned} P_{22} \quad & \int_{-1}^{1}\int_{-1}^{1} \sum_{I=1}^{4} N_{I,Y}\, \eta_{YI}\, t\, dX\, dY - \delta P_{EXT} = P_{22} \sum_{I=1}^{4} (-Y_I)\, \eta_{YI}\, t - \delta P_{EXT} \\ = \quad & \boldsymbol{\eta}^T \boldsymbol{G}_u = \boldsymbol{\eta}^T (\, \boldsymbol{R}_u - \boldsymbol{P}_{EXT}\,) = 0 \end{aligned} \tag{10.156}$$

with $\boldsymbol{R}_u^T = \{\, 0\,, -P_{22}\,, 0\,, -P_{22}\,, 0\,, P_{22}\,, 0\,, P_{22}\,\}\, t$.

In the same way, the explicit form of Eq. $(10.155)_2$ is given for $P_{22} = \text{const}$.

$$P_{22} \int_{-1}^{1}\int_{-1}^{1} \sum_{L=1}^{2} M_{L,Y}\, \delta\phi_L\, t\, dX\, dY = \delta\boldsymbol{\alpha}^T\, \boldsymbol{G}_\alpha = 0\,. \tag{10.157}$$

In this special situation $\boldsymbol{G}_\alpha^T = \{\, 0\,, 0\,, 0\,, 0\,\}$ follows from (10.153).

The solution of the nonlinear equations (10.156) and (10.157) follows usually by employing NEWTON'S method which needs the tangent matrix of the weak form. It is obtained from the general form, see e.g. (10.124), and can be stated explicitly for the square element Ω_e

$$\begin{aligned} \boldsymbol{K}_{u\,u} &= \begin{bmatrix} \boldsymbol{K}_{uu}^1 & \boldsymbol{K}_{uu}^2 \\ \boldsymbol{K}_{uu}^{2\,T} & \boldsymbol{K}_{uu}^1 \end{bmatrix} \quad \text{with} \\ \boldsymbol{K}_{u\,u}^1 &= \begin{bmatrix} 2a+2e & c+d & -2a+e & c-d \\ c+d & 2b+2e & -c+d & b-2e \\ -2a+e & -c+d & 2a+2e & -c-d \\ c-d & b-2e & -c-d & 2b+2e \end{bmatrix} t \\ \boldsymbol{K}_{u\,u}^2 &= \begin{bmatrix} -a-e & -c-d & a-2e & -c+d \\ -c-d & -b-e & c-d & -2b+e \\ a-2e & c-d & -a-e & c+d \\ -c+d & -2b+e & c+d & -b-e \end{bmatrix} t \\ \boldsymbol{K}_{\alpha\,u} &= \begin{bmatrix} 0 & \frac{4}{3}c & 0 & -\frac{4}{3}c & 0 & \frac{4}{3}c & 0 & -\frac{4}{3}c \\ \frac{4}{3}d & 0 & -\frac{4}{3}d & 0 & \frac{4}{3}d & 0 & -\frac{4}{3}d & 0 \\ 0 & \frac{4}{3}d & 0 & -\frac{4}{3}d & 0 & \frac{4}{3}d & 0 & -\frac{4}{3}d \\ \frac{4}{3}c & 0 & -\frac{4}{3}c & 0 & \frac{4}{3}c & 0 & -\frac{4}{3}c & 0 \end{bmatrix} t = \boldsymbol{K}_{u\,\alpha}^T \\ \boldsymbol{K}_{\alpha\,\alpha} &= \begin{bmatrix} 8a & 0 & 0 & 0 \\ 0 & 8e & 0 & 0 \\ 0 & 0 & 8e & 0 \\ 0 & 0 & 0 & 8b \end{bmatrix} t. \end{aligned} \tag{10.158}$$

The coefficients in these matrices are given by

$$\begin{aligned} a &= \frac{\mathbb{A}_{1111}}{6}; \qquad b = \frac{\mathbb{A}_{2222}}{6}; \qquad c = \frac{\mathbb{A}_{1122}}{4} = \frac{\mathbb{A}_{2211}}{4} \\ d &= \frac{\mathbb{A}_{1221}}{4} = \frac{\mathbb{A}_{2112}}{4}; \qquad\qquad e = \frac{\mathbb{A}_{1212}}{6} = \frac{\mathbb{A}_{2121}}{6}\,. \end{aligned}$$

Using block elimination within the solution of the linear equation system (10.124), the enhanced variables $\boldsymbol{\alpha}$ can be eliminated. With $\boldsymbol{K} = \boldsymbol{K}_{uu} - \boldsymbol{K}_{u\alpha}\,\boldsymbol{K}_{\alpha\alpha}^{-1}\,\boldsymbol{K}_{u\alpha}^{T}$, an equation system for the unknown displacements can be written as

$$\boldsymbol{K} = \boldsymbol{K}_{uu} - \begin{bmatrix} f & 0 & -f & 0 & f & 0 & -f & 0 \\ 0 & g & 0 & -g & 0 & g & 0 & -g \\ -f & 0 & f & 0 & -f & 0 & f & 0 \\ 0 & -g & 0 & g & 0 & -g & 0 & g \\ f & 0 & -f & 0 & f & 0 & -f & 0 \\ 0 & g & 0 & -g & 0 & g & 0 & -g \\ -f & 0 & f & 0 & -f & 0 & f & 0 \\ 0 & -g & 0 & g & 0 & -g & 0 & g \end{bmatrix} t \qquad (10.159)$$

where

$$f = \frac{2}{9}\left(\frac{d^2}{e} + \frac{c^2}{b}\right) \qquad g = \frac{2}{9}\left(\frac{d^2}{e} + \frac{c^2}{a}\right).$$

This relation constitutes the explicit structure of the element matrix for the homogeneous stress field with $P_{22} = \text{const.}$ at finite deformations. Specification of boundary conditions which are related to the homogeneous deformation, see Fig. 10. 3b, yields a further reduced matrix system.

For the computation of the eigenvector which is associated with the rank deficiency of the enhanced strain element, it is sufficient to consider only the nodal displacements $(u_2\,,\, u_3)$. The vertical displacements $(v_3 = v_4)$ follow from condition $P_{11} = 0$. Hence they are known values within the analysis. These considerations yield the nodal displacement vector for the element depicted in Fig. 10.3b: $\mathbf{v} = \{\,0\,,0\,,\mathrm{u}_2\,,0\,,\mathrm{u}_3\,,\mathrm{v}_3\,,0\,,\mathrm{v}_4\,\}$. Additionally, in case of a homogeneous stress state, it can be concluded: $\mathrm{u}_2 = \mathrm{u}_3$. However, both unknowns u_2 and u_3 have to be kept within the analysis; otherwise the *hour glass* form of the eigenvector cannot be detected.

The unknown increments of the enhanced variables $\Delta\boldsymbol{\alpha}$ follow from (10.125). Since $\boldsymbol{G}_\alpha = \mathbf{0}$ can be deduced from (10.157), it follows from (10.125) and the special structure of $\boldsymbol{K}_{u\,\alpha}$, see (10.158), that $\boldsymbol{\alpha}$ is generally zero for a homogeneous stress state.

The reduced form of (10.159) results from the specification of the boundary conditions

$$\boldsymbol{K} = \begin{bmatrix} 2a + 2e - f & a - 2e + f \\ a - 2e + f & 2a + 2e - f \end{bmatrix} t = \begin{bmatrix} A - f & B + f \\ B + f & A - f \end{bmatrix} t. \qquad (10.160)$$

A rank deficiency of $\boldsymbol{K}$ is present once the eigenvalue of the matrix are less or equal zero. The eigenvalues can be computed from $\boldsymbol{K} - \omega\, \boldsymbol{I}$ and are determined from

$$\frac{1}{t^2}\, \det\, (\boldsymbol{K} - \omega\, \boldsymbol{I}) = \omega^2 + 2\omega(f - A) + K\,, \quad \text{with } K = A^2 - B^2 - 2f(A + B)\,. \tag{10.161}$$

This yields

$$\omega_{1,2} = A - f \pm \sqrt{(A - f)^2 - K} \quad \Longrightarrow \quad \left\{ \begin{array}{ll} \omega_1 = & A + B \\ \omega_2 = & A - B - 2\, f\,. \end{array} \right. \tag{10.162}$$

The coefficients A, B and f depend upon the coefficients of the constitutive tensor (10.150) and also on the principal stretches λ_1 and λ_2. Since the normal stress P_{11} is equal to zero, which is also true for the principal stress P_1, it is possible to determine the stretch λ_2 as a function of λ_1

$$P_1 = 0 = \frac{1}{\lambda_1} \left[\mu\, (\lambda_1^2 - 1\,) + \frac{\Lambda}{2}\, (J^2 - 1) \right] \longrightarrow \lambda_2 = \frac{1}{\lambda_1} \sqrt{1 - \frac{2\mu}{\Lambda}\, (\lambda_1^2 - 1)}\,. \tag{10.163}$$

Now the eigenvalues ω_1 and ω_2 of the tangent matrix $\boldsymbol{K}_T$ can be written as a function depending on λ_1. Since

$$A + B = \frac{\mathbb{A}_{1111}}{2} = \mu + \frac{\Lambda}{2\, \lambda_1^2}, \tag{10.164}$$

the eigenvalue ω_1 is for $\mu > 0$ and $\Lambda \geq 0$ always positive. Thus the hour glass instability can only be observed by looking at the second eigenvalue

$$\hat{\omega}_2(\lambda_1) = A - B - 2f = \frac{1}{6}\mathbb{A}_{1111} + \frac{2}{3}\mathbb{A}_{1212} - \frac{1}{6} \left(\frac{\mathbb{A}_{1221}^2}{\mathbb{A}_{1212}} + \frac{\mathbb{A}_{1122}^2}{\mathbb{A}_{2222}} \right) < 0\,. \tag{10.165}$$

The function $\omega_2 = \hat{\omega}_2(\lambda_1)$ is shown in Fig. 10.4 for a value of the LÁME constant $\Lambda = 100.000$ and the shear modulus $\mu = 20$. As can be seen in Fig. 10.4, a negative eigenvalue ω_2 occurs for a stretch $\lambda_1 > 1.6344$. From (10.163), it follows that $\lambda_2 < 0.6116$.

The eigenvector associated with $\omega_2 = 0$ can be computed from $(\boldsymbol{K}_T - \omega_2\, \boldsymbol{1})\, \boldsymbol{\phi}_2 = \boldsymbol{0}$. With (10.158), (10.161) and (10.162), the eigenvector

$$\boldsymbol{\phi}_2^T = \{ \boldsymbol{\phi}^{u\,T}\,, \boldsymbol{\phi}^{\alpha\,T} \} = \{ 1\,, -1\,, 0\,, \alpha_\alpha\,, 0\,, \beta_\alpha\, \} \tag{10.166}$$

is obtained. In this result, the first two components are the displacements $\boldsymbol{\phi}^u$ in X-direction. The last four components belong to the enhanced modes $\boldsymbol{\phi}^\alpha$ with

$$\begin{aligned} \alpha_\alpha = \frac{d}{3\, e} &= \frac{1}{2}\, \frac{\mathbb{A}_{1221}}{\mathbb{A}_{1212}} = \frac{1}{2\, J} \left[1 + \frac{\Lambda}{2\, \mu}\, (\, 1 - J^2) \right] \\ \beta_\alpha = \frac{c}{3\, b} &= \frac{1}{2}\, \frac{\mathbb{A}_{1122}}{\mathbb{A}_{2222}} = \frac{1}{2}\, \frac{\lambda_2^2\, J}{\frac{\mu}{\Lambda}\, (\lambda_2^2 + 1) + \frac{1}{2}\, (J^2 + 1)}\,. \end{aligned} \tag{10.167}$$

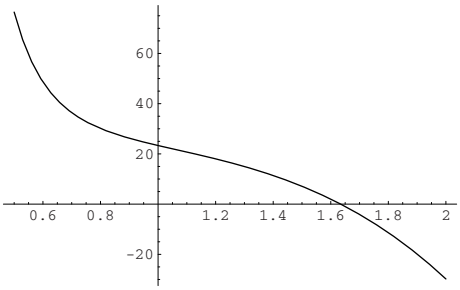

Fig. 10.4 Eigenvalue as function of the stretch λ_1

For the above selected values of Λ and μ, the eigenvectors follow which are, depicted in Fig. 10.5.

Remark 10.4:

1. In the linear elastic case, the stretches are $\lambda_1 \approx 1, \quad \lambda_2 \approx 1$. Then it follows from (10.165)
$$\hat{\omega}_2(1) = \frac{1}{6}\left(\Lambda - \frac{\Lambda^2}{\Lambda + 2\mu}\right) + \frac{5}{6}\mu\,.$$
The eigenvalue is for $\mu > 0$ always positive. Thus the hour-glassing described above does not occur.
2. The eigenvectors of the pure Q1-displacement element can be determined in the same way. In that case, f in (10.165) is equal to zero which yields
$$\omega_{1,2} = A \pm B \longrightarrow \begin{cases} \omega_1 = \frac{\mu}{2}(1 + \frac{1}{\lambda_1^2}) + \frac{\Lambda}{4\lambda_1^2}(J^2+1) > 0 \\ \omega_2 = \frac{\mu}{6}(5 + \frac{1}{\lambda_1^2}) + \frac{\Lambda}{12\lambda_1^2}(J^2+1) > 0\,. \end{cases}$$
Also in this case the hour-glass instability does not occur for parameters of the LÁME constants ($\mu > 0\,,\ \Lambda \geq 0$) which make physically sense.
3. It can be shown that the hour-glass instability does not depend on the material model. In Reese (1994) and Glaser and Armero (1997), the same effects were

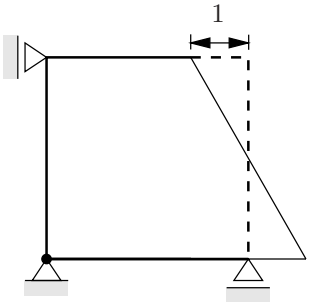

Fig. 10.5a X-component $\boldsymbol{\phi}^u$

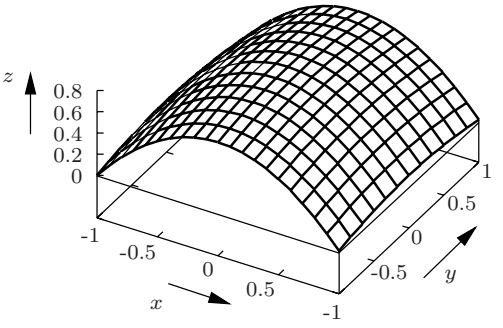

Fig. 10.5b Y-component $\boldsymbol{\phi}^\alpha$

observed for OGDEN materials. Furthermore, rank deficiency of the enhanced strain element was observed in de Souza Neto et al. (1995) for elasto-plastic deformations.

4. For the class of enhanced strain interpolations discussed in this section, hour-glass instabilities are only observed for pressure states since for $0 < \lambda_1 \leq 1$ no zero eigenvalue occurs, see Fig. 10.4.

The hour-glass modes discussed above can also be found when using standard enhanced strain elements for inhomogeneous stress states. The rank deficiency occurs only for elements which are situated in areas where compressive stresses occur.

10.5.5 Stabilization of the Enhanced Strain Formulation

Once the phenomenon was detected, different research groups started to work on methods to overcome instable behaviour of the enhanced strain elements. Within this research work different methods were developed. One method is related to classical hour-glass stabilization, as discussed in Sect. 10.4. Another technique is related to the choice of a different interpolation of the enhanced strains. A third method uses different strain energies within the enhanced formulation. These methods are discussed below.

Hour-Glass Stabilization. The *hour-glass* stabilization is performed as well for the displacements as for the enhanced modes. For the displacements, the stabilization can be obtained using γ-vectors as defined in (10.59). The two-dimensional form is presented in (10.95) explicitly. When additionally the eigenvectors, related to the enhanced modes, are stabilized then in the two-dimensional case the stabilization vectors

$$\begin{aligned} \bar{\boldsymbol{\gamma}}_1{}^T &= \{\gamma_1\,,0\,,\ldots\,,\gamma_4\,,0\,,0\,,\alpha_\alpha\,,0\,,\beta_\alpha\}\,, \\ \bar{\boldsymbol{\gamma}}_2{}^T &= \{0\,,\gamma_1\,,\ldots\,,0\,,\gamma_4\,,\alpha_\alpha\,,0\,,\beta_\alpha\,,0\} \end{aligned} \tag{10.168}$$

are obtained. Here α_α and β_α are defined by (10.167). The last four terms define the stabilization of the enhanced modes.

With these stabilization vectors, the incremental equation system for the unknowns $\boldsymbol{v}^T = \{\, \boldsymbol{u}^T\,, \boldsymbol{\alpha}^T \,\}$ can be written as

$$\left(\boldsymbol{K}_T + \sum_{s=1}^{2} c_s\, \bar{\boldsymbol{\gamma}}_s\, \bar{\boldsymbol{\gamma}}_s^T \right) \Delta \boldsymbol{v} = -\boldsymbol{G} - \sum_{s=1}^{2} c_s\, \bar{\boldsymbol{\gamma}}_s (\bar{\boldsymbol{\gamma}}_s^T\, \boldsymbol{v})\,, \tag{10.169}$$

see also (10.124) and (10.63). This equation system is solved as (10.126) by block-elimination.

This stabilization is only used when negative eigenvalues are found within an element. This requires for general quadrilaterals a generalized computation of the eigenvalues, see e.g. Glaser and Armero (1997). Here the problem is that the components of the eigenvector belonging to the enhanced modes depend upon the deformations, see (10.167). A simplified version for the

determination of the constants α_α and β_α follows from the computation of the constants for $\lambda_i \longrightarrow 1$ and $J \longrightarrow 1$

$$\alpha_\alpha = \frac{1}{2} \qquad \beta_\alpha = \frac{1}{2}\,\frac{\Lambda}{2\,\mu + \Lambda}\,. \tag{10.170}$$

This procedure was implemented in a two-dimensional Q1E4 element. For the basic formulation, see Simo and Armero (1992) or Wriggers and Hueck (1996) and Exercise 10.1. The resulting enhanced elements are rank deficient in compression states.

In order to investigate the influence of the described stabilization, a block under compression is considered under plane strain conditions. Its initial configuration is depicted in Fig. 10.6a for a finite element mesh with 16 × 16 elements. At the upper side, a constant vertical displacement is applied such that a constant stress state occurs. The constitutive parameters were selected as $\Lambda = 100.000$ and $\mu = 20$. The first physical eigenvector is shown in Fig. 10.6b. Convergence of the solution is obtained for a discretization with 64 × 64 elements. For this mesh the critical stretch, belonging to the physical eigenvector, is $\lambda_2 = 0.575$. Several computations were performed in order to investigate the dependency of the stabilization parameter on the solution. This also included a convergence study regarding the necessary mesh refinement. The computation of the system depicted in Fig. 10.6a yields a stretch λ_2 which belongs to the first physical eigenvector. This value is provided for the parameter c_s depending on the mesh refinement in Table 10.2. For comparison, the stretch which belongs to the first singularity of the non-stabilized enhanced element is documented in the first row of Table 10.2. The stretch belonging to the nonphysical hour-glass mode, see also Fig. 10.2b, is $\lambda_2 = 0.695$. This result is independent on mesh refinement, since the rank deficiency is a local phenomenon, see above. For the discretization with one element, the solution from Fig. 10.5a was used. It is different since in this special case different boundary conditions were employed.

It is clear from the values reported in Table 10.2 that the stabilization procedure avoids the hour-glass instability of the enhanced element. Furthermore, the solution only depends slightly upon the stabilization parameter c_s. The formulation converges to the stretch $\lambda_2 = 0.575$. For comparison reasons, the solution of the Q1-displacement element is reported too.

Table 10.2 Stretch λ_2 belonging to singularity

FEM	1x1	8x8	16x16	32x32	64x64
$c_s = 0$	0.612	0.695	0.695	0.695	0.695
$c_s = 10\,\mu$	0.260	0.475	0.555	0.575	0.580
$c_s = 100\,\mu$	0.245	0.470	0.550	0.570	0.575
$c_s = 1000\,\mu$	0.245	0.470	0.550	0.570	0.575
$c_s = 10000\,\mu$	0.245	0.470	0.550	0.570	0.575
Q1-Element	—	0.040	0.085	0.165	0.370

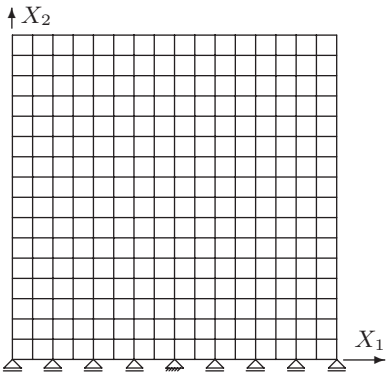

Fig. 10.6a FEM discretization

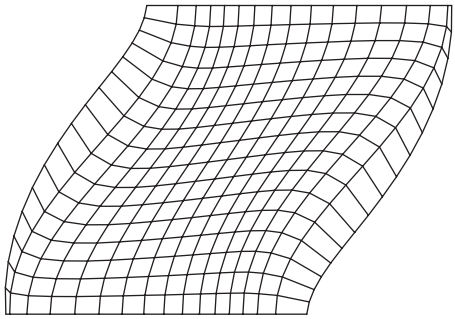

Fig. 10.6b 1st physical eigenvector

However it shows the locking of the displacement element which results from the quasi-incompressible material behaviour.

10.5.6 Special Interpolation of the Enhanced Modes

The rank deficiency occurs as well for distorted as for undistorted element geometries within the enhanced strain formulation. Hence a finite element formulation has to be developed which does not degenerate to a Q1E4 element.[6] In some cases, an interpolation of the enhanced modes can be constructed such that negative eigenvalues are avoided in (10.165). The associated formulation was presented in Korelc and Wriggers (1996b) and Glaser and Armero (1997). Starting from the two-dimensional formulation (10.79), the interpolation of the incompatible modes can be written in more general form as

$$\widehat{\boldsymbol{M}}(\boldsymbol{\xi})^{2D}\,\boldsymbol{\alpha} = \sum_{L=1}^{4} \boldsymbol{M}(\boldsymbol{\xi})_L^{2D}\,\alpha_L = \begin{bmatrix} \xi\,\alpha_1 & M_2(\xi\,,\eta)\,\alpha_2 \\ M_3(\xi\,,\eta)\,\alpha_3 & \eta\,\alpha_4 \end{bmatrix}. \qquad (10.171)$$

The interpolation on the main diagonal of $\boldsymbol{M}^{2D}$ cannot be changed in order to avoid volume locking. Korelc and Wriggers (1996a) developed orthogonality conditions for the ansatz polynomials M_{12} and M_{21} which resulted from the eigenvalue analysis (10.161). These were designed to avoid negative eigenvalues and hence rank deficiency. The conditions are

$$\begin{aligned} \int_{\Omega_e} M_2(\xi\,,\eta)\,M_3(\xi\,,\eta)\,d\Omega &= 0\,, \\ \int_{\Omega_e} M_2(\xi\,,\eta)\,d\Omega &= 0\,, \end{aligned} \qquad (10.172)$$

[6] Note that higher order integration does not solve the problem.

$$\int_{\Omega_e} M_3(\xi\,,\eta)\,d\Omega \quad = \quad 0\,.$$

The application of these conditions yield in the simplest case

$$\widehat{\boldsymbol{M}}(\boldsymbol{\xi})^{2D}\,\boldsymbol{\alpha} = \sum_{L=1}^{4} \boldsymbol{M}(\boldsymbol{\xi})^{2D}_{L}\,\alpha_L = \begin{bmatrix} \xi\,\alpha_1 & \xi\,\alpha_2 \\ \eta\,\alpha_3 & \eta\,\alpha_4 \end{bmatrix} = [\boldsymbol{M}(\boldsymbol{\xi})^{2D}]^T\,, \qquad (10.173)$$

which is the transpose of the interpolation in (10.79). With such interpolation, called CG4 or Q1/E4T, no instabilities occur in compression states, see Korelc and Wriggers (1996a) and Glaser and Armero (1997).[7]

However, this formulation (CG4 or Q1/E4T) is not totally free of singularities which can occur in the case of large elasto-plastic deformations in tension states and hence lead to rank deficiency of these enhanced strain formulations. This is also true for the three-dimensional formulation (CG9), which is based on the transposed of the interpolation matrix (10.80), see Korelc and Wriggers (1996b).

Additionally, several other approaches were proposed to stabilize the enhanced element formulation when applied to the numerical simulation of the finite deformation problems. Some of these methods are discussed below.

1. A possibility to avoid rank deficiency of the Q1/E4 element is provided by a change in the continuum formulation. Crisfield et al. (1995) have used the right stretch tensor $\mathbf{U}$ in the Hu–Washizu functional instead of the deformation gradient $\mathbf{F} = \mathbf{R}\,\mathbf{U}$. This however is not sufficient to prevent instabilities. Hence the authors have additionally evaluated the rotation tensor $\mathbf{R}$ only at the element mid point as in a co-rotational formulation. This element does not hour-glass in compression states. However, the formulation is quite complex since the rotation and the stretch tensor have to be determined and all constitutive equations must be provided for Biot stresses, see also Exercise 3.10. Furthermore, it seems that this formulation tends to lock in some applications.
2. de Souza Neto et al. (1996) developed an element which is based on an interpolation of the strains using a constant deformation gradient. This element depicts no rank deficiency but has several drawbacks. First, the formulation results in a non-symmetric tangent matrix - even for elastic materials - and second it locks in bending situations.
3. Another stabilization technique was developed by Glaser and Armero (1997) based on the Q1/E4T element. In this formulation, the authors add to the functional (10.64), after elimination of the stresses a stabilization term which acts on the volumetric part of the deformation

$$\mathit{\Pi}_{\alpha}(\boldsymbol{\varphi},\mathbf{F}) = \mathit{\Pi}(\boldsymbol{\varphi},\mathbf{F}) + \int_{B} \frac{\alpha}{2}\,[\,\det\mathbf{F} - 1\,]^2\,dV\,. \qquad (10.174)$$

[7] The CG4 and Q1/E4 interpolations cannot be distinguished in the linear theory, see Korelc and Wriggers (1996b).

This approach avoids hour glassing of the Q1/E4T or CG4 formulation under tension states if a small value for α / μ is selected, see Glaser and Armero (1997). A scheme, how to determine α depending on a problem at hand, is however not provided by the authors.

4. Bischoff et al. (1999b) employ least square methods using stabilization concepts known from work in the area of numerical flow simulations. With such techniques, the authors circumvent hour - glassing of the enhanced elements at finite deformation states. The stabilization is obtained via a deformation dependent function; however in the cited paper all results are valid only for rectangular elements.
5. Reese and Wriggers (2000) use the stability analysis discussed in the last section to develop a technique which automatically changes the element formulation such that hour glassing does not occur. In this approach, it is necessary to do the stability analysis for elements with arbitrary distorted geometries. Once an eigenvalue in (10.165) is equal zero or negative, the element formulation is changed such that instability is circumvented. Different cases have to be distinguished, for details see Reese and Wriggers (2000). These techniques have been successfully employed for three-dimensional simulations of finite elasto-plastic problems, see Reese (2003) and Reese (2005).

10.5.7 Special One Point Integration and Enhanced Stabilization

The enhanced variational methods provide a high flexibility for the generation of different finite elements. This will be shown by the following formulation in which an element will be derived which can be applied successfully to solid problems of finite elasticity and is based on a split of the element deformation into a homogeneous and inhomogeneous part, as introduced in Nadler and Rubin (2003) for the COSSERAT point element. It does not depict, as well as the COSSERAT point element, any nonphysical instabilities and does not rely on any analytical solutions. The difference is that simply the inhomogeneous part of the deformation is enhanced, as it is responsible for the locking behavior. Within this formulation, the deformation gradient $\mathbf{F}$, see (3.14), is additively split into its homogeneous and inhomogeneous part

$$\mathbf{F} = \bar{\mathbf{F}} + \widehat{\mathbf{F}} \,, \tag{10.175}$$

with

$$\bar{\mathbf{F}} = \frac{1}{V} \int_{\Omega} \mathbf{F} \, dV \tag{10.176}$$

being the volume average of the displacement gradient and V the element volume in the initial configuration. The strain energy density function is split accordingly, leading to

$$W(\mathbf{F}) = W_H \left(\bar{\mathbf{F}} \right) + W_I(\widehat{\mathbf{F}}) \,. \tag{10.177}$$

For the homogeneous part of the deformation, a compressible Neo–Hooke material introduced for the strain energy function W_H, see (3.116) with $g(J) = \frac{\Lambda}{2}\left(\bar{J}-1\right)^2$. Substituting the overall deformation measures by their homogeneous parts yields for the 1st PIOLA–KIRCHHOFF stresses

$$\bar{\mathbf{P}} = \frac{\partial W_H}{\partial \bar{\mathbf{F}}} = \Lambda \bar{J}\left(\bar{J}-1\right)\bar{\mathbf{F}}^{-T} + \mu\left(\bar{\mathbf{F}} - \bar{\mathbf{F}}^{-T}\right), \tag{10.178}$$

where

$$\bar{J} = \det\left(\bar{\mathbf{F}}\right) \text{ and } \bar{\mathbf{C}} = \bar{\mathbf{F}}^T\,\bar{\mathbf{F}}$$

are the volume averaged values of the deformation gradient, the JACOBIAN and the right CAUCHY–GREEN tensor, respectively.

For the inhomogeneous part of the element deformation, the strain energy density function is defined by a linear elastic model model, see (3.121), since the inhomogeneous deformation part consists mainly of bending and torsion deformations, see Nadler and Rubin (2003), which can be described well by this model.

$$W_I(\widehat{\mathbf{H}}) = \frac{1}{2}\widehat{\mathbf{H}} \cdot \mathbb{C}_0\left[\,\widehat{\mathbf{H}}\,\right] \tag{10.179}$$

with a constant elasticity tensor $\mathbb{C}_0$, see (3.272). The 1st PIOLA–KIRCHHOFF stress tensor is then given by

$$\widehat{\mathbf{P}} = \Lambda \mathrm{tr}(\widehat{\mathbf{H}})\mathbf{1} + \mu\left(\,\widehat{\mathbf{H}} + \widehat{\mathbf{H}}^T\,\right). \tag{10.180}$$

Now the inhomogeneous part of the displacement gradient is enhanced such that

$$\widehat{\mathbf{H}} = \tilde{\mathbf{H}} + \hat{\mathbf{H}} \tag{10.181}$$

where

$$\tilde{\mathbf{H}} = \mathbf{H}\left(\boldsymbol{\varphi}\right) - \bar{\mathbf{H}} \tag{10.182}$$

is the displacement gradient following from the deformation and $\hat{\mathbf{H}}$ is the enhanced displacement gradient.

By using the above definitions, the HU–WASHIZU functional (10.64) can be rewritten as

$$\mathit{\Pi}\left(\boldsymbol{\varphi}, \hat{\mathbf{H}}, \mathbf{P}\right) = \int_{\Omega}\left[W_H(\bar{\mathbf{H}}) + W_S(\widehat{\mathbf{H}}) - \widehat{\mathbf{P}} \cdot \hat{\mathbf{H}}\right] dV - P_{ext} = 0\,. \tag{10.183}$$

The variation of Eq. (10.183) w.r.t. its independent variables $\boldsymbol{\varphi}$, $\hat{\mathbf{H}}$ and $\mathbf{P}$ leads to

$$\begin{aligned}
\int_{\Omega} \delta\bar{\mathbf{H}} \cdot \frac{\partial W_H}{\partial \bar{\mathbf{F}}}\, dV + \int_{\Omega} \delta\tilde{\mathbf{H}} \cdot \frac{\partial W_S}{\partial \widehat{\mathbf{H}}}\, dV - \delta P_{ext} &= 0, \\
\int_{\Omega} \delta\hat{\mathbf{H}} \cdot \left(\frac{\partial W_S}{\partial \widehat{\mathbf{H}}} - \widehat{\mathbf{P}}\right) \mathrm{d}V &= 0, \\
\int_{\Omega} \delta\widehat{\mathbf{P}} \cdot \hat{\mathbf{H}}\, dV &= 0.
\end{aligned} \tag{10.184}$$

Equation $(10.184)_1$ yields the standard weak form of the equilibrium and Eq. $(10.184)_2$ the constitutive equation. In a weak sense, Eq. $(10.184)_3$ provides an orthogonality condition between the stress tensor and the displacement gradient. Hence the finite element interpolations for the enhanced displacement gradient have to be chosen such that the orthogonality conditions

$$\int_{\Omega} \delta\hat{\mathbf{H}} \cdot \widehat{\mathbf{P}}\, dV = 0, \qquad \int_{\Omega} \delta\widehat{\mathbf{P}} \cdot \hat{\mathbf{H}}\, dV = 0 \tag{10.185}$$

are fulfilled. Then, Eqs. (10.184) become

$$\begin{aligned} \int_{\Omega} \delta\bar{\mathbf{H}} \cdot \frac{\partial W}{\partial \bar{\mathbf{F}}}\, dV + \int_{\Omega} \delta\tilde{\mathbf{H}} \cdot \frac{\partial W}{\partial \widehat{\mathbf{H}}}\, dV - \delta P_{ext} &= 0, \\ \int_{\Omega} \delta\hat{\mathbf{H}} \cdot \frac{\partial W}{\partial \widehat{\mathbf{H}}}\, dV &= 0\,. \end{aligned} \tag{10.186}$$

These equations are the basis for the subsequent development of the enhanced finite element formulation.

Finite Element Discretization. A standard finite element discretization is employed within a single element Ω_e where the position of a material point in the current configuration $\boldsymbol{\varphi}$ is approximated by trilinear isoparametric shape functions

$$\boldsymbol{\varphi}^h = \sum_{I=1}^{n} N_I \boldsymbol{\varphi}_I = \sum_{I=1}^{n} N_I \left(\boldsymbol{X}_I + \boldsymbol{u}_I\right), \tag{10.187}$$

where $\boldsymbol{X}_I$ are the positions of the nodes of Ω_e with respect to the initial configuration and $\boldsymbol{u}_I$ are the nodal displacements. The formulation is presented here for an eight-node brick element as shown in Fig. 4.8. For the interpolation functions N_I standard trilinear shape functions, defined in (4.40), are used.

With the transformation, see also (4.44),

$$\frac{\partial N_I}{\partial \boldsymbol{X}} = \boldsymbol{J}^{-T} \frac{\partial N_I}{\partial \xi}, \tag{10.188}$$

where $\boldsymbol{J} = \frac{\partial \boldsymbol{X}}{\partial \xi}$ is the standard JACOBIAN of the isoparametric map and (ξ, η, ζ) are the coordinates of the point ξ in the reference configuration, the displacement gradient can be written as

$$\mathbf{H}^h = \begin{bmatrix} H^h_{11} \\ H^h_{22} \\ H^h_{33} \\ H^h_{12} \\ H^h_{21} \\ H^h_{23} \\ H^h_{32} \\ H^h_{13} \\ H^h_{31} \end{bmatrix} = \sum_{I=1}^{8} \boldsymbol{B}_I \, \boldsymbol{u}_I \quad \text{with} \quad \boldsymbol{B}_I = \begin{bmatrix} N_{I,X} & 0 & 0 \\ 0 & N_{I,Y} & 0 \\ 0 & 0 & N_{I,Z} \\ N_{I,Y} & 0 & 0 \\ 0 & N_{I,X} & 0 \\ 0 & N_{I,Z} & 0 \\ 0 & 0 & N_{I,Y} \\ N_{I,Z} & 0 & 0 \\ 0 & 0 & N_{I,X} \end{bmatrix} . \tag{10.189}$$

The discrete form of the homogeneous part of the displacement gradient is obtained by inserting Eq. (10.189) into Eq. (10.176), leading to

$$\bar{\mathbf{H}}^h = \frac{1}{\Omega_e} \int_{\Omega_e} \mathbf{H}^h \, d\Omega = \sum_{I=1}^{8} \frac{1}{\Omega_e} \int_{\Omega_e} \boldsymbol{B}_I \, d\Omega \, \mathrm{u}_I = \sum_{I=1}^{8} \bar{\boldsymbol{B}}_I \, \boldsymbol{u}_I \, . \tag{10.190}$$

Note that a numerical integration over the element volume can be avoided in this equation by using the ansatz functions introduced by Belytschko et al. (1984) which allow an analytical integration.

With Eqs. (10.189) and (10.190), the discrete form of the inhomogeneous part of the displacement gradient $\tilde{\mathbf{H}}$ is written as

$$\tilde{\mathbf{H}}^h = \sum_{I=1}^{8} \left(\boldsymbol{B}_I - \bar{\boldsymbol{B}}_I \right) \, \boldsymbol{u}_I = \sum_{I=1}^{8} \tilde{\boldsymbol{B}}_I \, \boldsymbol{u}_I \, . \tag{10.191}$$

For the enhanced displacement gradient $\tilde{\mathbf{H}}$, the ansatz functions have to be chosen such that they fulfil the orthogonality condition given in Equations (10.185). Here, three quadratic functions are used to interpolate the enhanced modes, as introduced in Wilson et al. (1973)

$$M_1 = \left(1 - \xi^2\right) \quad M_2 = \left(1 - \eta^2\right) \quad M_3 = \left(1 - \zeta^2\right) \, . \tag{10.192}$$

Then, the enhanced displacement gradient can be discretized on the element level as

$$\hat{\mathbf{H}}^h = \begin{bmatrix} \hat{H}^h_{11} \\ \hat{H}^h_{22} \\ \hat{H}^h_{33} \\ \hat{H}^h_{12} \\ \hat{H}^h_{21} \\ \hat{H}^h_{23} \\ \hat{H}^h_{32} \\ \hat{H}^h_{13} \\ \hat{H}^h_{31} \end{bmatrix} = \sum_{L=1}^{3} \boldsymbol{G}_L \boldsymbol{\alpha}_L \quad \text{with } \boldsymbol{G}_L = \begin{bmatrix} M_{L,X} & 0 & 0 \\ 0 & M_{L,Y} & 0 \\ 0 & 0 & M_{L,Z} \\ M_{L,Y} & 0 & 0 \\ 0 & M_{L,X} & 0 \\ 0 & M_{L,Z} & 0 \\ 0 & 0 & M_{L,Y} \\ M_{L,Z} & 0 & 0 \\ 0 & 0 & M_{L,X} \end{bmatrix} \tag{10.193}$$

and $\boldsymbol{\alpha}_L$ are the enhanced variables,

$$\boldsymbol{\alpha}_L^T = [\alpha_{1L}\,, \alpha_{2L}\,, \alpha_{3L}]\,. \tag{10.194}$$

Linearization and Solution Procedure. With the help of Eqs. (10.190), (10.191) and (10.193), the discrete form of the variational equations (10.186) is given by

$$\begin{aligned} \bigcup_{e=1}^{n_e} \left(\sum_{I=1}^{8} \delta \boldsymbol{u}_I^T \bar{\boldsymbol{B}}_I^T \bar{\boldsymbol{P}}\, \Omega_e + \sum_{I=1}^{8} \delta \boldsymbol{u}_I^T \int_{\Omega_e} \tilde{\mathbf{B}}_I^T \widehat{\mathbf{P}}\, d\Omega \right) - \delta P_{\mathrm{EXT}} &= 0 \\ \sum_{K=1}^{3} \delta \boldsymbol{\alpha}_K^T \int_{\Omega_e} \boldsymbol{G}_K^T \mathbb{C}_0 \left[\tilde{\boldsymbol{H}}^h \right] d\Omega &= 0 \end{aligned} \tag{10.195}$$

where Eq. $(10.195)_2$ is defined on the element level. This leads to the nodal residual vectors within an element Ω_e

$$\begin{aligned} \boldsymbol{R}_I^u &= \bar{\boldsymbol{B}}_I^T \bar{\boldsymbol{P}}^h\, \Omega_e + \int_{\Omega_e} \tilde{\boldsymbol{B}}_I^T \widehat{\boldsymbol{P}}^h \,\mathrm{d}\Omega - \boldsymbol{P}_I^{EXT}, \\ \boldsymbol{R}_L^\alpha &= \int_{\Omega_e} \tilde{\boldsymbol{B}}_I^T \mathbb{C}_0 \tilde{\boldsymbol{H}}^h \,\mathrm{d}\Omega, \end{aligned} \tag{10.196}$$

where $\boldsymbol{P}_I^{EXT}$ is the nodal vector related to the external loads. The linearization of equations (10.195) yields on element level

$$\begin{aligned} \boldsymbol{K}_{IJ}^{uu} &= \bar{\boldsymbol{B}}_I^T \mathbb{D} \bar{\boldsymbol{B}}_J\, \Omega_e + \int_{\Omega_e} \tilde{\boldsymbol{B}}_I^T \mathbb{C}_0 \tilde{\boldsymbol{B}}_J \,\mathrm{d}\Omega \\ \boldsymbol{K}_{IL}^{u\alpha} &= \int_{\Omega_e} \tilde{\boldsymbol{B}}_I^T \mathbb{C}_0 \boldsymbol{G}_L \,\mathrm{d}\Omega \\ \boldsymbol{K}_{KJ}^{\alpha u} &= \int_{\Omega_e} \boldsymbol{G}_K^T \mathbb{C}_0 \tilde{\boldsymbol{B}}_J \,\mathrm{d}\Omega \\ \boldsymbol{K}_{KL}^{\alpha\alpha} &= \int_{\Omega_e} \boldsymbol{G}_K \mathbb{C}_0 \boldsymbol{G}_L \, d\Omega \quad . \end{aligned} \tag{10.197}$$

With Eqs. (10.195) and (10.197), the system of linear equations which has to be solved in every NEWTON iteration can be constructed by standard assembly, see Sect. 4.2. Here, as discussed already in Sect. 10.5.2, a block elimination of the variables $\boldsymbol{\alpha}$ can be obtained based on the linear system on element level, for details see Exercise 10.1.

This element is called Q1/EI9 due to the fact that standard tri-linear ansatz functions are used to interpolate the volume averaged and the enhanced part and that additionally nine enhanced modes are applied to describe the small strain elastic enhanced stabilization part.

10.6 Examples

The performance of the different elements is shown by means of examples suitable to point out important properties of the different elements such as high coarse mesh accuracy, low mesh distortion sensitivity and locking free response for bending and incompressibility dominated problems. Furthermore, it can be shown that some of the elements do not hour-glass for arbitrary problem classes and loading.

The element formulation which are compared in this section are standard isoparametric as well as special elements for good bending performance and for incompressible problems. The following elements were selected:

- two standard elements Q1 and Q2 which use tri-linear and tri-quadratic interpolations, respectively, see Sect. 4.2,
- the mixed Q1/P0 element as proposed by Simo et al. (1985a) for finite deformations, see also Sect. 10.2.1,
- the classical enhanced element QM1/E12, developed in Simo et al. (1993b), and
- the Q1/EI9 element described in the last section.

All elements use a hyperelastic material model, see (3.116) with $g(J) = \frac{A}{2}\left(\bar{J}-1\right)^2$.

10.6.1 Patch Test

The patch test proposed by MacNeal and Harder (1985) is used for a displacement patch test. The the finite element mesh is shown in Fig. 10.7(a). Boundary conditions are set such that a rotation around the x_3-axis is possible, but no other rigid body motion. A displacement in the x_2-direction is applied at point P, resulting in a rotation around the x_3-axis. All elements fulfil this patch test; hence the computed stresses are zero. For the traction controlled patch test, the same mesh is used. The nodes at $x_1 = 0$, $x_2 = 0$ and $x_3 = 0$ are fixed in the x_1-direction, x_2-direction and x_3-direction, respectively. A surface load is applied in the x_1-direction, see Fig. 10.7(b). This configuration should lead to a uniform stress σ_{11}, while all other stresses should be zero. The force patch test is fulfilled by all elements except for the QM1/E12.

10.6.2 Beam with Distorted Mesh

A cantilever beam of length l, width $2\,w$ and height h is loaded with an equally distributed shear force $F = 12\,\mathrm{N}$ at its free end, as shown in Fig. 10.8. The boundary conditions are such that the clamped end is fixed in the

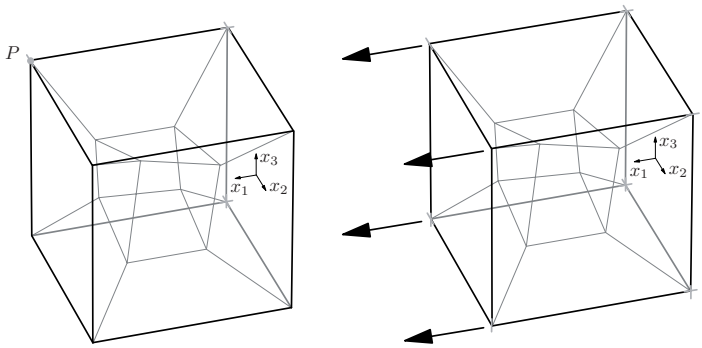

Fig. 10.7 (**a**) displacement and (**b**) force patch test

x_1-direction. Additionally, the node at $x_1 = x_2 = x_3 = 0$ is fixed in the x_2-direction to avoid rigid body motion. All nodes at $x_3 = 0$ are fixed in the x_3-direction. Due to the loading, the rectangular cross section and the boundary conditions, symmetry conditions can be enforced. In order to circumvent a stress singularity at the clamped end, the shear load is applied there in the opposite direction instead of fixing these points in the x_2-direction. The geometry and the material data of the beam as well as the load applied and the boundary conditions are provided in Fig. 10.8.

The convergence of the deflection v_P in x_2-direction of point P depicted in Fig. 10.8 is investigated for the Q1/EI9 element as well as the Q1, Q2 and QM1/E12 element. Four different meshes are used, with $16 \times 4 \times 2$,$32 \times 8 \times 4$, $64 \times 16 \times 8$ and $128 \times 32 \times 16$ elements, respectively.

In Table 10.3, the displacement v_P in x_2-direction of point P is depicted for all elements, as a function of the number of degrees of freedom. As expected, the Q1 element locks. Both enhanced strain elements are softer than the Q2 element, where the QM1/E12 is closer to the Q2 element than the Q1/EI9 element. This shows the good coarse mesh accuracy of the enhanced elements. As expected, all elements converge to the same solution. For better visualization, only the results for the elements which do not lock are shown in Fig. 10.9 where the displacement v_P is plotted for the Q1/EI9, the Q2 and

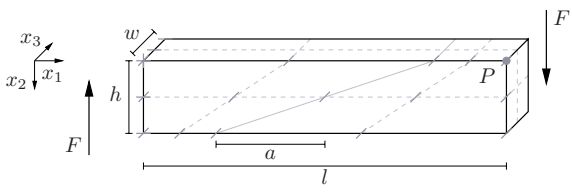

Fig. 10.8 Beam: system, load and material data

Table 10.3 Beam with distorted mesh: Displacement v_P [mm] for the Q1/EI9, Q1, Q2 and QM1/E12 element

Degrees of freedom	Q1/EI9	Q1	Q2	QM1/E12
664	1.0379	0.5778	1.0128	1.0299
4112	1.0314	0.7840	1.0257	1.0279
28576	1.0283	0.9358	1.0270	1.0273
28576	1.0275	1.0007	1.0271	1.0272

the QM1/E12 with respect to the number of elements. The pure displacement element Q2 converges from below, as the mathematical theory predicts. Both mixed elements, QM1/E12 and Q1/EI9, converge from above.

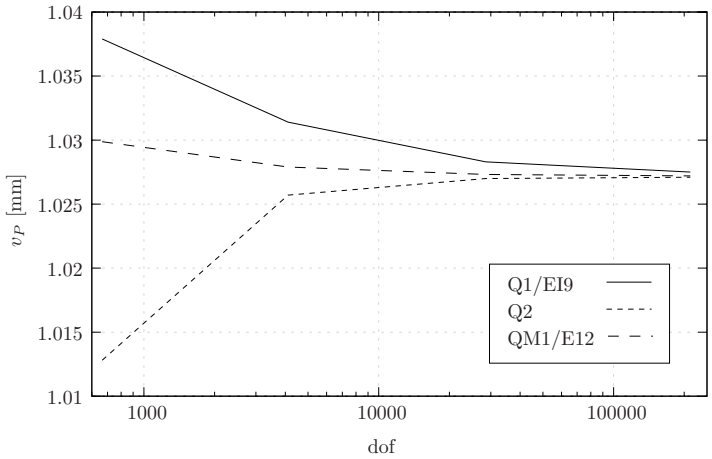

Fig. 10.9 Beam with distorted mesh: Displacement v_P for the Q1/EI9, Q2 and QM1/E12 element

10.6.3 Nearly Incompressible Block

A nearly incompressible block of length l, width w and height h is loaded by an equally distributed surface load q at its top centre, as shown in Fig. 10.10. Furthermore, all nodes on the top of the block are fixed in the x_1- and x_2-directions. For symmetry reasons, only a quarter of the block is discretized. The bottom face of the block is fixed in the x_3-direction. The symmetry boundary conditions are set such that nodes at $x_1 = 0.5\,w$ are fixed in x_1-direction and nodes at $x_2 = 0.5\,l$ are fixed in x_2-direction. These boundary conditions are chosen according to a similar test presented in Reese et al. (2000).

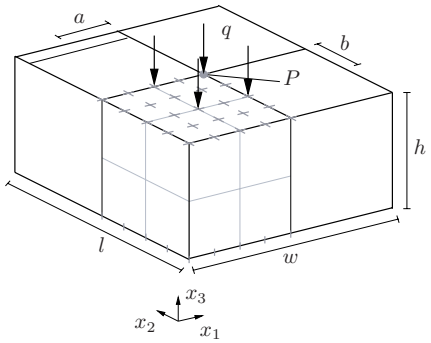

Geometry
$h = 50\,\text{mm}$
$w = 100\,\text{mm}$
$l = 100\,\text{mm}$
$a = 25\,\text{mm}$
$b = 25\,\text{mm}$

Load
$q = 3\,\text{MPa}$

Material
$\Lambda = 499.92568\,\text{MPa}$
$\mu = 1.61148\,\text{MPa}$

Fig. 10.10 Nearly incompressible block: system, load and material data

The geometry and the material as well as the applied load and the boundary conditions are provided in Fig. 10.10. The convergence of the vertical displacement w_P in x_3-direction at the point P, in Fig. 10.10, is investigated for the Q1/EI9 and the Q1, Q2, Q1P0 and the QM1/E12 element for regular meshes with $4 \times 4 \times 4$, $8 \times 8 \times 8$, $16 \times 16 \times 16$, $32 \times 32 \times 32$ and $64 \times 64 \times 64$ elements.

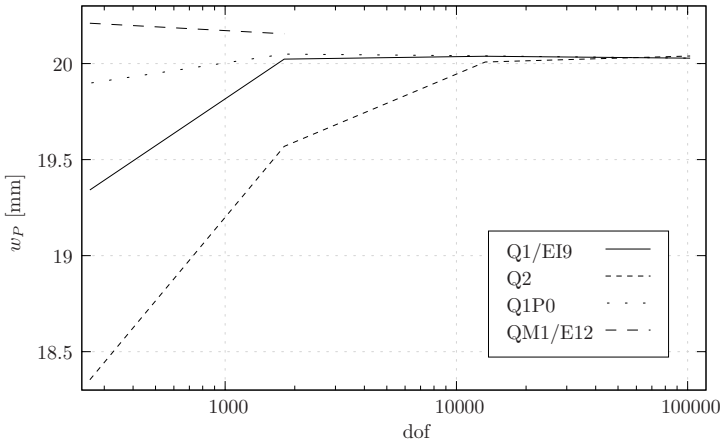

Fig. 10.11 Nearly incompressible block: Displacement w_P for the Q1/EI9, Q2, Q1P0 and QM1/E12 element

In Table 10.4, the vertical displacement w_P in x_3-direction of point P is shown as a function of the number of degrees of freedom for all elements. It can be observed that the Q1 element locks, as can be expected for this nearly incompressible problem. Both enhanced strain elements and the Q1P0 element are softer than the Q2 element. Thus still mild locking occurs for the higher order quadratic displacement element. Again, all elements except the QM1/E12 element converge to the same solution. For the QM1/E12 element,

Table 10.4 Nearly incompressible block: Displacement w_P [mm] for the Q1/EI9, Q1, Q2, Q1P0 and QM1/E12 element

Degrees of freedom	Q1/EI9	Q1	Q2	Q1P0	QM1/E12
260	19.342	7.656	18.354	19.898	20.2097
1800	20.023	13.083	19.569	20.049	20.1549
13328	20.038	17.492	20.008	20.040	
102432	20.028	19.493	20.040	20.028	
802880	20.025	19.951	20.026	20.025	

solutions can only be obtained for the two coarsest meshes. For finer mesh resolutions, the QM1/E12 element depicts nonphysical hour-glass instabilities. The displacement w_P are plotted for the Q1/EI9, Q2, Q1P0 and QM1/E12 element in Fig. 10.11 to visualize the results for the elements that are known to perform well for this test. It can be seen that the Q1P0 and the Q1/EI9 element perform extremely well, even for very coarse meshes. The Q2 element converges slower which is related to a mild locking of this element.